JOURNAL OF CATALYSIS 127, 141–166 (1991)

Molecular Orbital Studies of the Adsorption of CH_3, CH_2, and CH on Rh(111) and Ni(111) Surfaces

A. DE KOSTER AND R. A. VAN SANTEN[1]

Laboratory for Inorganic Chemistry and Catalysis, Eindhoven University of Technology, P.O. Box 513, 5600 MB Eindhoven, The Netherlands

Received December 21, 1989

The adsorption of methyl (CH_3), methylene (CH_2), and methyne (CH) is studied on Rh(111) and Ni(111) with the atom superposition and electron delocalization (ASED) and extended Hückel molecular orbital methods. Results are analyzed by calculating the local density of states (LDOS) and bond order overlap populations. On Rh(111) CH is adsorbed on threefold sites, CH_2 on twofold sites and CH_3 on onefold sites in order to restore missing C–H bonds. The height of CH_x to the metal surface decreases with decreasing hydrogen content x, while the adsorption energy increases. Adsorption of CH_3 on Rh(111) is studied in detail. CH_3 bonds on the metal surface mainly via σ type interactions of the n CH_3 orbital with surface metal atoms of the same symmetry. In case of the onefold adsorption, the highest occupied molecular orbital (n CH_3) has a large interaction with metal s, p_z, and d_{z^2} orbitals. For twofold adsorption it interacts mainly with the symmetric s, p_x, and d_{xz} metal group orbitals. Interactions of surface metal orbitals with the π and π^* orbitals are weak. Preliminary results are presented for the coupling reaction of coadsorbed CH_2 and CH_3. A strong repulsion due to steric interaction of the hydrogen atoms is found when the carbon–carbon distance is decreased. As a result the direct coupling reaction of CH_3 and CH_2 does not seem to be a suitable reaction path for the C–C coupling reaction. In a final section we have analyzed CH_3 adsorption on Ni(111). With parameters implying a large spatial extension of the d orbitals, CH_3 is found to adsorb on onefold sites. Decreasing the spatial extension of the Ni d orbitals causes a shift to multiply bonding adsorption sites. This illustrates the subtle balance between the interaction with the s valence electrons that favor high coordination sites and the interaction with the d valence electrons favoring low coordination sites.

INTRODUCTION

In the Fischer–Tropsch process, synthesis gas is converted into hydrocarbons. Suitable catalysts are Ni, Co, Rh, Ru, and Fe. Several different mechanisms have been proposed to describe the formation of hydrocarbons. We mention the carbide mechanism (*1, 2*), the dehydrocondensation model (*2, 3*), the carbon monoxide insertion model (*4, 5*), and the CH_x insertion model (*6–12*).

In the carbide model (*1, 2*), adsorbed CO dissociates into C_{ad} and O_{ad} and the oxygen-atom reacts with hydrogen or CO to give a surface carbide, which is hydrogenated into alkanes. According to the dehydrocondensation mechanism (*2, 3*), adsorbed CO is first partially hydrogenated into HCOH. Two adsorbed HCOH or RCOH species recombine (chain growth) by splitting of the C–O bond under elimination of water. In the CO insertion model (*4, 5*) CO inserts into a metal–hydrogen or metal–alkyl bond (chain growth) followed by hydrogenolysis. The "CH_x model" (*8, 10, 13–19*) is generally accepted now as the main mechanism. The hydrocarbon synthesis consists of initiation, propagation, and termination elementary steps.

According to the CH_x insertion model, the first step in the Fischer–Tropsch process (initiation step) is the dissociation of hydrogen and carbon monoxide, and the formation of CH_x groups:

$$H_2 + \bullet \rightarrow 2H^*$$

[1] To whom correspondence should be addressed.

0021-9517/91 $3.00

$$CO + \bullet \rightarrow CO^*$$

$$CO^* \rightarrow C^* + O^*$$

$$C^* + xH^* \rightarrow CH_x^* + x\bullet \quad x = 1 - 3.$$

Longer chain products are formed by insertion of CH_x^* (propagation step):

$$CH_x^* + C_nH_{2n+1}^* \rightarrow C_{n+1}H^*_{2n+1+x}.$$

Reaction is ended (termination step) by hydrogenation leading to paraffins

$$C_nH^*_{2n+1} + H^* \rightarrow C_nH_{2n+2}$$

by β-hydrogen abstraction (leading to olefins)

$$C_nH^*_{2n+1} \rightarrow C_nH_{2n} + H^*$$

or the formation of oxygenates by CO insertion

$$C_nH^*_{2n+1} + CO \rightarrow C_nH_{2n+1}CO^* \rightarrow C_{n+1-OxO}.$$

The adsorption of CO on transition metal surfaces has been extensively studied with quantum chemical methods. Both extended Hückel (*20–29*) and ab initio methods (*30–34*) have been used. Theoretical studies of CO dissociation on metal surfaces are rather scarce. Yin-Sheng and Xiao-Le have studied CO dissociation on supported Rh and Ni with the extended Hückel method (*35*). In our laboratory we studied adsorption (*36*) and dissociation of CO on the (111), (100), and (110) surfaces of Rh (*37*) and Ni(111) (*38*). Here we report studies on the chemisorption of CH_x fragments.

Only a limited number of studies of adsorption and reaction of hydrocarbon fragments on metal surfaces are reported in the literature. Acetylene (C_2H_2) has attracted attention because experiments suggested rearrangement to either ethylidyne (CCH_3) or vinylidene (CCH_2). LEED intensity analysis data have been published of Ni(111) P(2 × 2) C_2H_2 (*39*), Pt(111) P(2 × 2) C_2H_3 (*40*), and Rh(111) (2 × 2) C_2H_3 (*41*). Other techniques used are high-resolution electron energy loss spectroscopy (HREELS) and thermal desorption spectrometry (TDS) (*42*).

Stewart and Ehrlich (*43*) have studied the activated adsorption of methane on Rh with field emission and molecular beam techniques. Dissociative adsorption is activated by about 7 kcal/mol.

Silvestre and Hoffmann (*44*) studied in detail C_2H_n on Pt(111). Anderson *et al.* have studied the adsorption and dissociation of acetylene (*45–47*), adsorption and α-hydrogen abstraction of propylene (C_3H_6) on Pt(111) (*48*), and the selective oxidation of methane on MoO_3 (*49*). Gavezzoti *et al.* (*50, 51*) have studied the adsorption of acetylene and fragments (CH, C–C, C–C–H, H_2CC, H_3CC, and H_3CCH) on Pt(111) with extended Hückel methods. The extended Hückel studies have been proven to be useful to predict adsorption geometries in agreement with LEED measurements (*47, 51*) and reactivity of metal surfaces to acetylene (*45*).

Ab initio studies are few. Geurts and van der Avoird (*52*) have used Hartree–Fock–Slater-LCAO to study the interaction of C_2H_2 with Ni(111). Different adsorption sites and adsorption geometry of C_2H_2 and surface specific dissociation on (small) Ni clusters have been investigated, and theoretical results (shift in UPS ionization energy, C–C stretch frequency) have been related to experimental ones. Nakatsuji *et al.* (*53*) studied the hydrogenation of acetylene using ab initio methods. The adsorption of CH_x (x = 1,2,3) fragments on metal surfaces has been studied by several groups. Minot *et al.* (*54*) have studied CH_n and C–CH_n adsorption on Pt(111) and Zheng *et al.* (*55*) report a detailed study of CH_n adsorption on Ti, Cr, and Co surfaces. CH_3 adsorption on Ni(100) (*56*) and Ni(111) (*57*) has been studied with ab initio methods.

Hoffmann and co-workers have studied the reaction path of methyl migration in $CH_3Mn(CO)_5$ as a model of the carbonylation reaction (*58*), a comparison of H–H and C–H bond activation in transition metal complexes and on surfaces (*59*), and migration of CH, CH_2, and CH_3 on metal surfaces (*55*). In the same paper calculations are reported on combination reactions of hydro-

carbon fragments. Calculations are presented for the combination of two CH_3 fragments (termination reaction), CH_3 + CH_2 (chain propagation to ethene), and CH_2 + CH_2 (chain propagation to ethylene). Baetzold (*60*) published results of a kinetic model of hydrocarbon formation from H_2 and CO. A completely different approach is followed by Shustorovich and Bell (*61, 62*), who use the bond order conservation model.

The adsorption site of CH_x is still controversial. Minot *et al.* (*54*) found with the extended Hückel method that on Pt(111) CH is adsorbed on threefold sites, CH_2 on twofold sites, and CH_3 on onefold sites. Similar results are reported by Zheng *et al.* (*55*) for CH_x adsorption on Ti, Cr, and Co. In contrast with this are calculations of CH_3 on Ni(111). Extended Hückel calculations of Gavin *et al.* (*63*) and ab initio results of Siegbahn and co-workers (*57*) indicate a preference of CH_3 for the three fold hollow site.

The preferential adsorption site of CH_3 on different metals might be found by establishing the differences in electronic structure. In particular, the relative importance of the metal *s* and *d* electrons is likely to play a role. We have studied the adsorption of CH_n (n = 1,2,3) on Rh(111) and Ni(111) with the atom superposition and electron delocalization (ASED) method. In this method, the total energy is found by a summation of the attractive energy as calculated with the extended Hückel method, and a repulsive energy term. This gives us the advantages of the extended Hückel method, and we can analyze bonding in a straightforward way by using the concepts of local density of states (LDOS) and bond order overlap populations and densities. We apply these concepts to analyze one- and twofold adsorption of CH_3.

One of the disadvantages of the extended Hückel method is that a reliable geometry optimization is not possible, and experimental data must be used for bond lengths and bond distances if available. In case of adsorption of hydrocarbons, these values are not known except in the case of C_2H_2 adsorption (*39–41*). In the ASED method geometry optimization is possible to some extent and we have optimized the heights of adsorbing hydrocarbon fragments. It also gives us an opportunity to calculate the energy of intermediate steps of reactions, and determine the most probable reaction path as we have done for CO dissociation in a previous study (*37*).

The extended Hückel method is parameter dependent in contrast to the ab initio methods. However, this can be used as an advantage and one can study the trends occurring upon variation of parameters. In our study of CH_3 adsorption on Ni(111) we have used this approach to study the influence of the spatial extension of Ni *d* orbitals on the adsorption of CH_3.

THEORETICAL METHOD AND CLUSTER MODELS USED

In the atom superposition and electron delocalization molecular orbital method (*64, 65*), the total energy E_{tot} is calculated by a summation of an attractive and a repulsive energy

$$E_{tot} = E_{att} + E_{rep}. \tag{1}$$

The repulsive energy E_{rep} is an approximate expression derived from an analysis of corrections due to the electron–electron interactions (*65*). The attractive energy E_{att} is found by applying extended Hückel molecular orbital techniques (*66, 67*). Parameters used are listed in the Appendix. In the tables E_{tot} and E_{att} are separately listed.

Local density of states and bond order overlap densities have been used in analyzing changes in electronic structure. The LDOS is calculated with

$$\rho_{ii}(E) = \sum_k |\langle \Phi_i | \Psi_k \rangle|^2 \, \delta(E - E_k) \tag{2}$$

with Φ_i the fragment orbital and Ψ_k the calculated molecular orbital.

Bond order overlap densities are calculated with

$$\pi_{ij}(E) = \sum_k \mathrm{Re}\, c_i^{*k} c_j^k S_{ij} \, \delta(E - E_k). \tag{3}$$

c_i^k is the coefficient of fragment orbital i in molecular orbital k and S_{ij} is the overlap between the fragment orbitals. The integral of the bond order overlap curve up to the Fermi level is the total overlap population of the specified bond. The Fermi level is indicated relative to the vacuum level. In all plots, calculated $\rho_{ii}(E)$ and $\pi_{ij}(E)$ are presented after convolution with a Gaussian distribution (σ = 0.25 eV).

The Rh(111) surface is modeled by an (18,11) two-layer model as described earlier (*36*). Atoms in the center of this cluster are fully coordinated by six Rh atoms in the same layer and three Rh atoms in the second layer. All adsorption and reaction studies involve those central atoms. The Rh–Rh internuclear distance is taken equal to the bulk value of 2.687Å (*68*). The Ni(111) surface is modeled by the same cluster model with a Ni–Ni distance of 2.4916 Å (*68*). Studies involving two adsorbates (e.g., the coadsorption of CH_2 and CH_2) are performed with a (24,16) two-layer cluster.

The C–H bond distance is optimized for gas phase CH_4 in steps of 0.001 Å to be 1.192 Å, while the H–C–H bond angle is kept fixed in the sp^3 hybridization (109°28′). This optimal C–H bond distance is kept constant in all studies of (adsorbed) CH_x. The metal surface is in the xy plane, adsorption takes place in the (positive) z direction.

Removing one hydrogen atom of CH_4 and leaving the rest of the molecule intact produces CH_3. The C–H bond of the removed hydrogen is aligned along the z-axis, and the remaining three hydrogen atoms are pointing away from the surface as their C–H bond makes an angle of 109° with the negative z-axis.

In adsorbed CH_2 an sp^2 geometry with the H–C–H bond angle of 120° is used. Both hydrogen atoms and carbon are in a plane perpendicular to the metal surface. The hydrogen atom of CH is pointing away from the surface in the z-direction.

The adsorption geometry of CH_x (x = 0 – 3) and H is found by a general optimization procedure. In a first step the adsorption height is optimized in steps of 0.1 Å by looking for a minimum of the ASED total energy E_{tot}. In a subsequent step the adsorbed molecule is rotated along the surface-carbon axis in steps of 10°. By taking the energy difference of the highest and lowest adsorption energy during rotation, the activation energy for rotation E_{rot} is found. At the optimum rotation angle the adsorption height is varied again as a check that the optimum adsorption height is not changed by rotation.

RESULTS AND DISCUSSION

Adsorption of CH_x on Rh(111)

Results of adsorption of CH_x and H are presented in Table 1. Both the ASED total energy E_{tot} and the extended Hückel energy E_{att} are given. Also included in Table 1 are the optimized adsorption height h_x and, for CH_2 and CH_3, the rotation energy barrier.

The number of hydrogen atoms x of CH_x has a marked influence on the adsorption energy and geometry. Adsorption energies are lowest for CH_3 and highest for CH. The adsorption energy of C is comparable with that of CH on the same site, measured by E_{tot}. The extended Hückel method predicts comparable adsorption energies for the one- and twofold sites, but it gives higher values for adsorption on the threefold sites of C than for adsorption of CH. Calculated adsorption energies obtained here are comparable with those in other theoretical studies. Schüle *et al.* (*57*) have found with ab initio methods values of 1.86–2.08 eV (43–48 kcal/mol) and 1.99–2.15 eV (46–50 kcal/mol) for CH_3 on the one- and threefold adsorption sites of Ni(111). Shustorovich and Bell (*62*) have calculated heats of adsorption with the bond order conservation model, and find values of 38–62 kcal/mol (1.65–2.69 eV) for CH_3, 68–104 kcal/mol (2.95–4.51 eV) for CH_2 and 97–142 (4.20–6.15 eV) for CH.

Table 2 compiles preferred adsorption sites and adsorption energies (E_{tot} and E_{att}) for these sites. Whereas C and CH prefer

TABLE 1

Adsorption of CH_x on a Rh(*18,11*) Cluster Modeling a (111) Surface

Species	Site	E_{tot} (eV)	E^a_{att} (eV)	E^b_{rot} (eV)	h^c_x (Å)
H	1-fold	−4.06	−4.91		1.6
	2-fold	−3.79	−4.72		1.1
	3-fold fcc[d]	−3.76	−4.58		1.0
	3-fold hcp[e]	−3.69	−4.51		1.0
C	1-fold	−4.43	−6.49		1.8
	2-fold	−4.88	−6.85		1.4
	3-fold fcc[d]	−5.48	−8.08		1.2
	3-fold hcp[e]	−5.58	−8.19		1.2
CH	1-fold	−4.52	−6.58		1.8
	2-fold	−4.96	−6.92		1.4
	3-fold fcc[d]	−5.53	−7.39		1.3
	3-fold hcp[e]	−5.53	−7.39		1.3
CH_2	1-fold	−3.40	−4.61	0.05	1.9
	2-fold	−3.78	−4.68	1.43	1.6
	3-fold fcc[d]	−3.22	−4.19	0.11	1.5
	3-fold hcp[e]	−3.21	−4.18	0.11	1.5
CH_3	1-fold	−2.54	−2.95	0.01	2.1
	2-fold	−1.85	−2.14	0.02	1.9
	3-fold fcc[d]	−1.72	−1.92	0.14	1.9
	3-fold hcp[e]	−1.72	−1.92	0.10	1.9

[a] Bond energy contribution excluding the two-body repulsion term.

[b] Difference in maximum and minimum total energy during rotation.

[c] Height of adsorbing species (X = C, H, or CH_x) above the surface.

[d] No Rh present in second layer.

[e] Rh present in second layer.

threefold sites, CH_2 is adsorbed on a twofold and CH_3 on a onefold site. The height of adsorption h_x decreases with decreasing hydrogen content x. Again, in the case of adsorption of C and CH, comparable adsorption heights are found.

Summarizing the results, we see that the adsorption energy is highest for CH and decreases with increasing hydrogen content x. This is related to a shift from the threefold to a lower coordination site and to an increase in the height h of the adsorbed CH_x. These trends are also found by Zheng *et al.* (*55*) and Minot *et al.* (*54*). Zheng *et al.* have used a fixed M–C distance of 2.1 Å, resulting in adsorption heights h_x of 2.1 Å (onefold), 1.61 Å (twofold), and 1.42 Å (threefold). Since the metal–carbon bonds are stronger than carbon–hydrogen bonds, adsorption on a higher coordination site results in a higher adsorption energy. Carbon tends to achieve a maximum coordination of 4. In the adsorbed CH_x, there are $(4 - x)$ carbon–hydrogen bonds missing and carbon will restore these missing bonds by bonding with an appropriate number of metal atoms. CH_x is therefore adsorbed on a $(4 - x)$ fold site. Since the metal–carbon bonds are stronger than carbon–hydrogen bonds, adsorption on a higher coordination site results in a higher adsorption energy and a shorter bond distance.

In Fig. 1 the adsorption energy (E_{att}) is shown as a function of the number of valence electrons. This correlation is found by variation of the number of valence electrons of the metal atoms (the number of valence electrons of Rh is 9) and assuming a "rigid band." Parameters and surface geometry are from Rh, and only the number of valence electrons is varied. Both adsorption energy (Figs. 1a, 1c, and 1e) and the ratio of adsorption energy to that of the preferred site on Rh(111) (Figs. 1b, 1d, and 1f) are shown. The ratio of adsorption energy of site x relative to the preferred site y is denoted as $E(xf/yf)$. In the case of CH (Figs. 1a and 1b) threefold adsorption sites are favored re-

TABLE 2

Preferred Adsorption Sites on Rh(111)

Atom	Site	E_{tot} (eV)	E_{att} (e)
H	1-fold	−4.06	−4.91
C	3-fold hcp	−5.58	−8.19
CH	3-fold [(1)]	−5.53	−7.39
CH_2	2-fold	−3.78	−4.68
CH_3	1-fold	−2.54	−2.95

[a] Same adsorption energy found for threefold fcc and hcp sites.

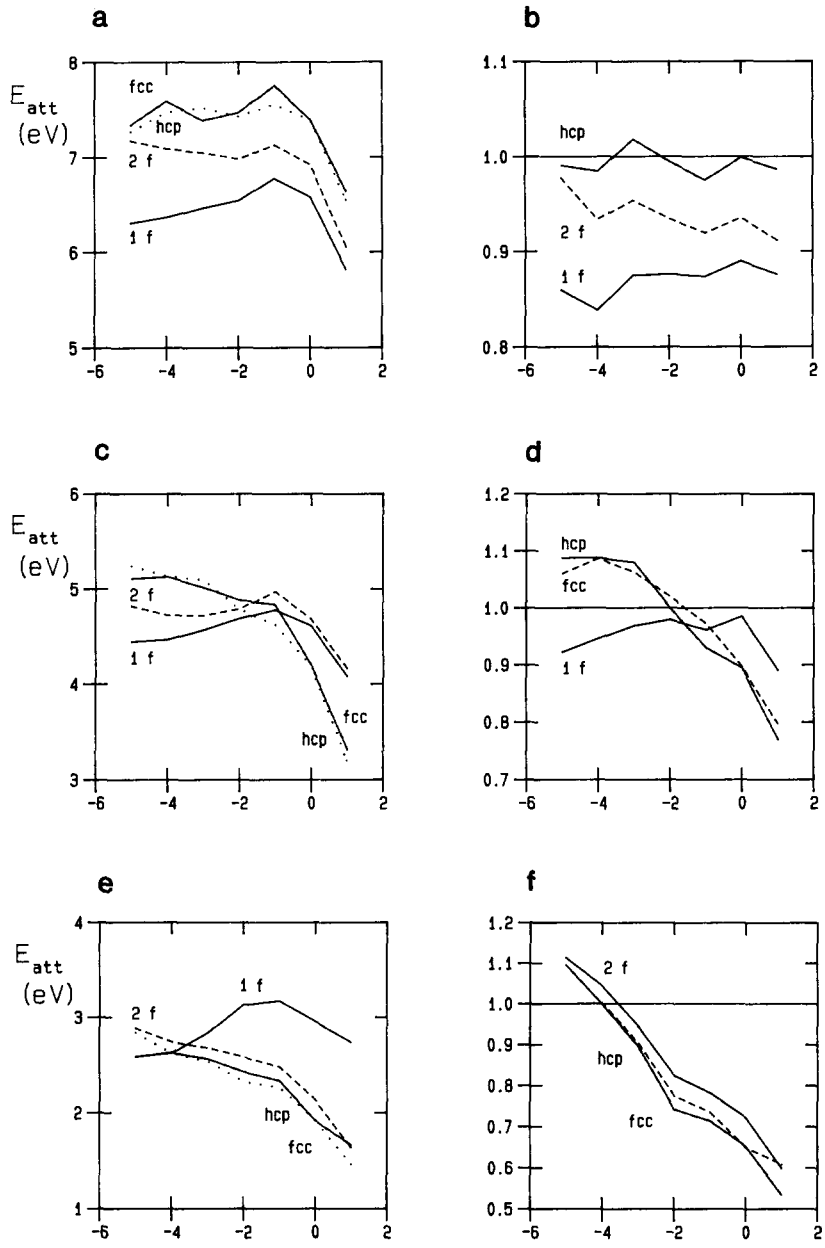

FIG. 1. Adsorption energy (E_{att}) and ratio of adsorption energy on an x-fold site to that of the preferred y-fold site ($E(xf/yf)$) of CH_x (x = 1,3) on (111) surface as a function of number of metal valence electrons per atm compared to Rh (0). (a) E_{att} of CH adsorbed one-, two-, threefold fcc and threefold hcp sites. (b) The ratio of the adsorption energy of CH adsorbed on one- and twofold sites relative to that of CH adsorbed on threefold sites. (c) E_{att} of CH_2 adsorbed one-, two-, threefold fcc and threefold hcp sites. (d) The ratio of the adsorption energy of CH_2 adsorbed on one- and threefold sites relative to that of CH_2 adsorbed on twofold sites. (e) E_{att} of CH_3 adsorbed one-, two-, threefold fcc and threefold hcp on sites. (f) The ratio of the adsorption energy of CH_3 adsorbed on two- and threefold sites relative to that of CH_3 adsorbed on onefold sites.

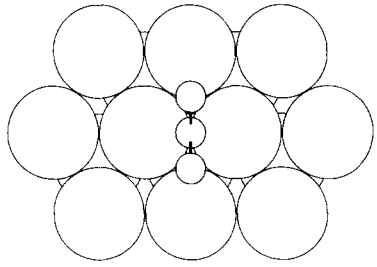

FIG. 2. The optimum geometry of CH_2 adsorbed on a twofold site on Rh(111).

gardless of the position of the Fermi level. The adsorption energy for the one- and twofold sites is always lower than that for the threefold sites, but $E(2f/3f)$ is slowly decreasing and $E(1f/3f)$ is slowly increasing. The difference in adsorption energy of the threefold fcc and hcp sites is negligible.

CH_2 favors adsorption on threefold sites when the Fermi level is low (Fig. 1c). The adsorption energy of threefold sites decreases at higher energy, while that of onefold and twofold sites increases. At a valence electron occupation of Ru twofold sites are preferred. At high Fermi levels all adsorption energies are decreased but twofold adsorption is still preferred but the energy difference with onefold sites becomes small. This is reflected in the ratios of adsorption energies (Fig. 1d). $E(3f/2f)$ both for threefold fcc and hcp sites is steadily decreasing from about 1.1 to 0.8. $E(1f/2f)$ increases to almost unity.

In the case of adsorption of CH_3 the onefold sites are clearly favored, except for very low Fermi levels (Fig. 1e). The adsorption energy for onefold sites increases at higher E_F energy, the adsorption energy of the two- and threefold sites decreases. The adsorption energy ratios (Fig. 1f) of the two- and threefold sites relative to onefold sites are steadily decreasing.

The energy barriers of CH_3 rotation are negligible for adsorption on the one- and twofold sites, and they are very small for the threefold sites. Since CH_3 is preferentially adsorbed on the onefold sites, rotation is little hindered by an energy barrier and CH_3 can be adsorbed in any conformation with respect to the surface metal atoms.

In the case of CH_2 very small rotation barriers are found for adsorption on the one- and threefold sites, but rotation on the preferred twofold site has a considerable energy barrier of 1.43 eV. The optimum geometry is found for hydrogen atoms staggered with respect to the surface Rh atoms with which the CH_2 fragment is bonded (Fig. 2). The plane through C and both hydrogen atoms is standing perpendicularly to the plane through carbon and both surface Rh atoms. The maximum of the rotation barrier is found when the hydrogen atoms, carbon, and both Rh atoms are in one plane and the hydrogen atoms are pointing toward the surface atoms (staggered). The hydrogen atoms form with C a yz plane which is perpendicular to an xz plane formed by the two surface Rh atoms and carbon. Considering the high rotation energy barrier there is a strong preference for this rectangular geometry.

Adsorption of CH_3 on Rh(111): Electronic Effects

The molecular orbital diagram of CH_3 is shown in Fig. 3. According to the Frontier

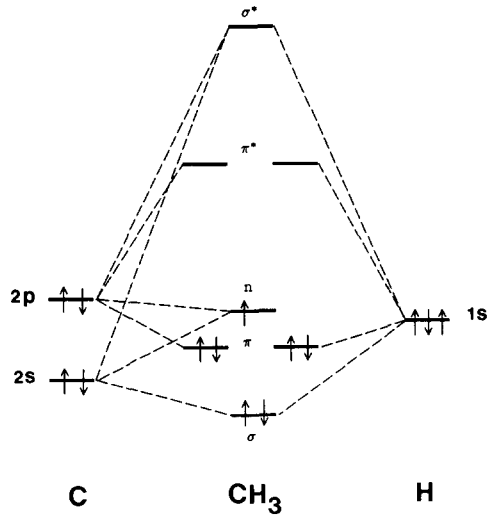

FIG. 3. Molecular orbital scheme of CH_3.

orbital concept (*69–72*) bonding is a result of interactions involving the highest occupied molecular orbital (HOMO) and the lowest unoccupied molecular orbital (LUMO). The HOMO of CH_3 is the n CH_3 orbital at -11.65 eV; the LUMO is a degenerated π^* orbital and found at 4.88 eV. It is expected that the π orbitals at -16.08 eV and the σ^* orbital at 21.50 eV are not involved in bonding.

The σ orbital is a bonding combination of the s orbital of C with the s orbitals of the three hydrogen atoms. The degenerate π orbitals are a combination of the carbon p_x orbital with two hydrogen s orbitals, and of the p_y orbital with three hydrogen s orbitals, respectively. The HOMO is the n CH_3 orbital, which is mainly a combination of the carbon s and p_z orbitals. Since the hydrogen orbitals hardly contribute to the n CH_3 orbital, this orbital is nonbonding in CH_3. The n CH_3 orbital is symmetric with respect to the metal surface. The two antibonding π^* orbitals are the LUMO. One of them is a combination of the carbon p_x with two hydrogen s orbitals; the other a combination of the p_y orbital with three hydrogen s orbitals. Since the two degenerate π^* orbitals are a combination of a carbon p orbital with a different number of hydrogen s orbitals they have a different symmetry with respect to the xz and yz mirror planes. The σ^* orbital is an antibonding combination of the s and p_z orbitals of carbon and the s orbitals of all three hydrogen atoms.

In Fig. 4 contour plots of the wave functions are given for the π^* and n CH_3 orbitals. The coordinates of CH_3 adsorbed onefold are used, and the contour plots on the metal surface (xy plane) are given. The contour plots therefore reflect the wave functions of CH_3 on the metal surface. In the xy plane the n CH_3 orbital (Fig. 4a) has a threefold rotation symmetry with respect to the z-axis (C_{3v}). This is a result of the small contribution of the hydrogen s orbitals and is therefore dependent on the relative positions of the three hydrogen atoms. These positions are quite arbitrary since the rotation of CH_3 has an almost zero energy barrier. According to the coordinates of hydrogen atoms used in this study, n CH_3 is perfectly symmetric with respect to the yz plane but slightly asymmetric with respect to the xz plane. The atom positions are indicated in Fig. 4.

Figure 4b shows the contour plot of the π^* orbital, which is a combination of p_x and two hydrogen s orbitals. This orbital is perfectly antisymmetric with respect to the yz plane. There is a considerable asymmetry with respect to the yz plane. The second π^* orbital is plotted in Fig. 4c. This orbital is a combination of the carbon p_y orbital with all three hydrogen s orbitals. As a result it is perfectly symmetric with respect to the yz plane.

When CH_3 is adsorbed on a metal surface, orbitals of CH_3 will interact with orbitals of the metal surface. Important in this process are the symmetry, relative energies and atomic gross populations of orbitals of adsorbate and surface. The Fermi level of Rh is calculated to be -10.99 eV. As a result, the d band will be filled considerably, while the s and p band will be nearly empty. This is confirmed by calculations of atomic orbital gross populations of metal orbitals before interaction with an adsorbate (Table 3a).

Surface metal orbitals will interact with adsorbate orbitals when interacting orbitals have the same symmetry and the difference in energy is small. Therefore we expect that metal orbitals will mainly interact with the half-filled n CH_3 orbital at -11.65 eV. As discussed above, the n CH_3 orbital is symmetric and will interact with metal orbitals which also are symmetric (the s, p_z, and d_{z^2} orbitals in the case of onefold adsorption). Interaction of the completely filled π orbitals (at -16.08 eV) and the completely empty π^* orbitals (at $+4.88$ eV) with surface metal orbitals will be small. Since the π CH_3 orbitals are completely filled in the gas phase CH_3, interaction with (partially) filled metal orbitals will result in repulsion. Interaction with metal orbitals is only possible in cases where electrons can be donated to the sur-

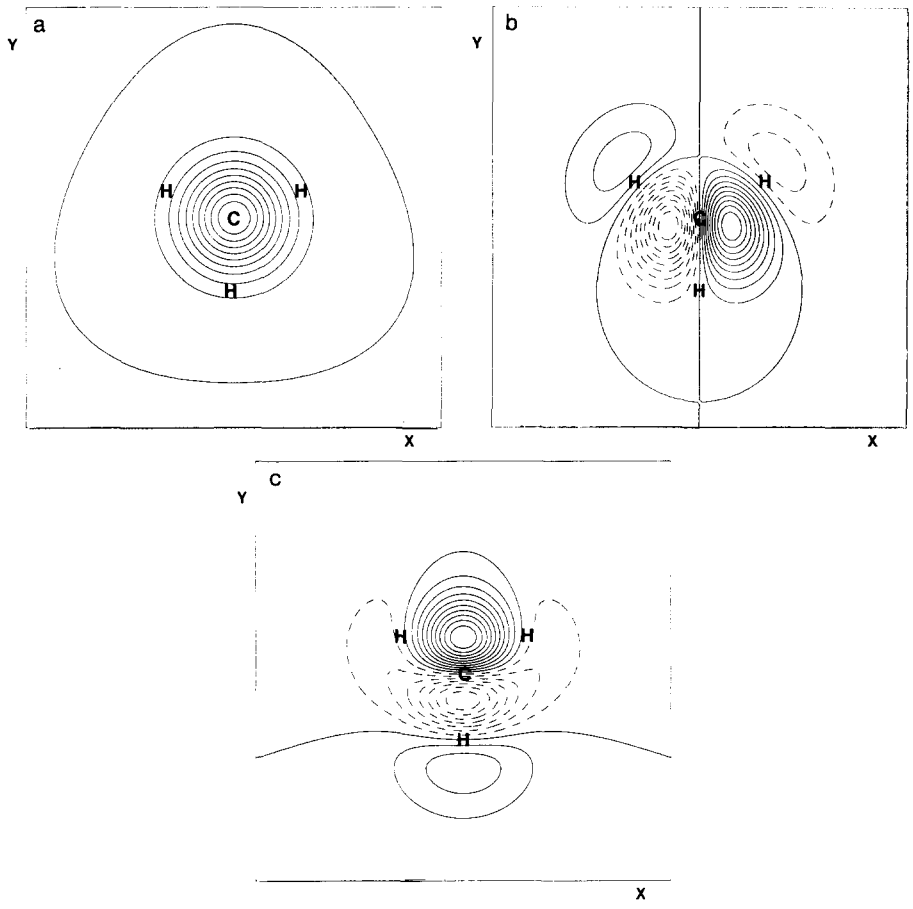

FIG. 4. Contour plots of molecular orbitals of CH_3. Indicated are the position of the carbon and hydrogen atoms of CH_3. (a) n CH_3 orbital, plotted in the xy plane. (b) π^* orbital which is antisymmetric with respect to the yz mirror plane, plotted in the xy plane. (c) π^* orbital which is symmetric with respect to the yz mirror plane, plotted in the xy plane.

face. The interaction of the π^* orbitals with metal orbitals will be small because of the large energy difference between interacting orbitals. The π and π^* orbitals of CH_3 will interact with metal surface orbitals which are antisymmetric (the p_x, p_y, d_{xz}, and d_{yz} orbitals in case of onefold adsorption). Changes in occupation of metal orbitals (Table 3a) are discussed in a later section.

The LDOS of the π, n CH_3, and π^* CH_3 orbitals for gas phase CH_3 and CH_3 adsorbed one- and twofold is presented in Fig. 5, and the gross populations are given in Table 3b. The density peak of the π CH_3 orbitals hardly broadens upon adsorption and it is found at a constant position, indicating that the π orbitals hardly interact with the metal surface. The gross population is hardly changed from 1.0 to 0.998 for onefold adsorption and 0.994 for twofold adsorption. These changes are of the same order of magnitude as changes in the density of the π orbitals of CO upon adsorption, and justify our approach to study only processes involving HOMO (the n CH_3 orbital) and LUMO (the π^* orbitals).

The LDOS of the n CH_3 orbital (Fig. 5b) is split into two peaks. One peak is shifted to lower energy as part of a bonding interaction, the other is shifted to higher energy

TABLE 3a

Surface atomic orbital gross populations: CH_3 on Rh(111)

	Orbital	1-fold	2-fold	
			σ	π
Before adsorption	s	0.293	0.327	0.270
After adsorption		0.460	0.485	0.285
Before adsorption	p_x	0.162	0.163	0.167
After adsorption		0.168	0.232	0.168
Before adsorption	p_y	0.162	0.154	0.177
After adsorption		0.167	0.156	0.177
Before adsorption	p_z	0.113	0.115	0.113
After adsorption		0.304	0.207	0.174
Before adsorption	$d_{x^2-y^2}$	0.802	0.939	0.647
After adsorption		0.802	0.906	0.640
Before adsorption	d_{z^2}	0.922	0.940	0.885
After adsorption		0.710	0.915	0.745
Before adsorption	d_{xy}	0.801	0.863	0.720
After adsorption		0.801	0.856	0.715
Before adsorption	d_{xz}	0.891	0.948	0.804
After adsorption		0.869	0.815	0.787
Before adsorption	d_{yz}	0.885	0.900	0.861
After adsorption		0.863	0.880	0.853

Note. In the case of twofold adsorption, CH_3 is adsorbed on a site consisting of two Rh atoms aligned along the x-axis and perpendicular to the surface along the z-axis. σ and π indicate symmetry and antisymmetry with respect to the yz mirror plane.

and is part of an antibonding interaction. As can be seen in Fig. 5b, more density is found in the bonding peak and the gross population of the n CH_3 orbital is increased from 0.5 to 0.744 for onefold adsorption. This increase in population of the n CH_3 orbital is also found by Zheng *et al.* (*55*) for CH_3 adsorption on Co(0001), Cr(110), and Ti(0001). In going from the onefold to the twofold adsorption sites both the bonding peak and the antibonding peak broaden and the n CH_3 orbital is slightly depopulated relative to onefold adsorption (gross population of 0.703).

The LDOS of the π^* orbitals is shifted to higher energy (Fig. 5c). This shift is larger for the twofold than for the onefold adsorption. Because of the broadening some density is below Fermi level, and these levels are therefore occupied. However, the increase in population of the π^* orbitals is small (0.011 and 0.012 for the onefold and twofold adsorption, respectively). This increase in population is much smaller than the increase of the $2\pi^*$ orbitals of CO upon adsorption (*36*), which is easily explained by the energy difference of the Fermi level of the Rh surface (at -10.99 eV) and the LUMO of the adsorbate. Whereas the density peak of the $2\pi^*$ orbitals of gas phase CO is found at -7.71 eV (energy difference with the metal Fermi level of 3.28 eV), the density of the π^* orbitals of CH_3 is found at 4.88 eV (energy difference: 15.87 eV). The larger the energy difference between two interacting orbitals, the smaller this interaction will be (*70*).

As the energy difference between the Fermi level of the metal and the π orbitals is large, their interaction will be small and bonding of CH_3 is mainly due to σ type interactions of the n CH_3 orbital with metal surface orbitals. Calculated bond order overlap populations for onefold and twofold adsorption of CH_3 are given in Table 4. We explain onefold adsorption first and rationalize results on the basis of symmetry. The symmetry of the (metal) atomic orbitals is well known; the symmetry of the the π^* and n orbitals of CH_3 is given above.

The n CH_3 orbital is symmetric with respect to the yz plane. Interaction with surface metal orbitals which are antisymmetric with respect to the yz plane (the p_x, d_{xz}, and d_{xy} orbitals) will be zero. The n CH_3 orbital is almost symmetric with respect to the xz plane. As the s, p_z, and d_{z2} orbitals are symmetric with respect to the x plane (and are symmetric with respect to the xz plane) they will have a strong interaction with the n CH_3

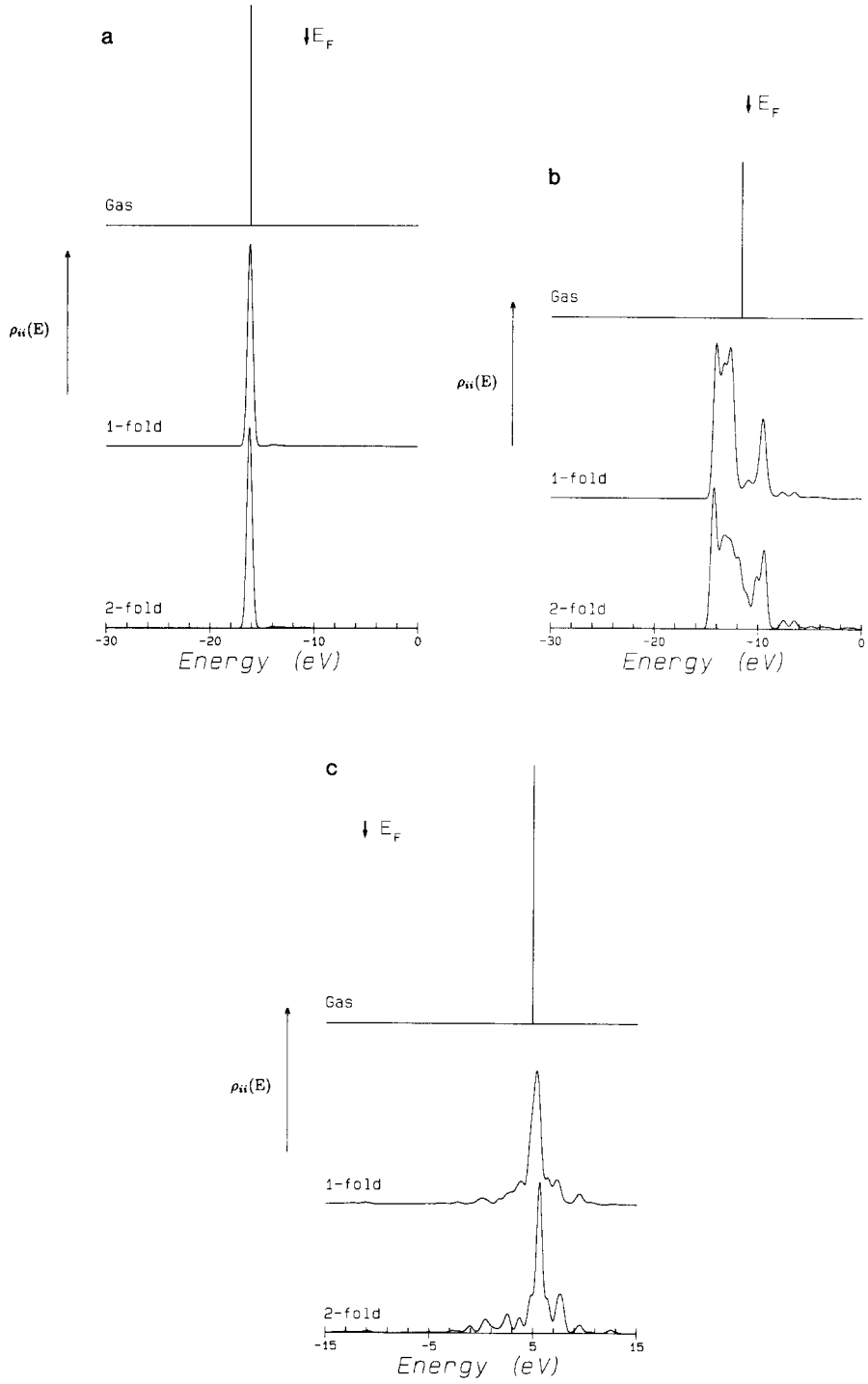

FIG. 5. LDOS of the π CH_3 (a), n CH_3 (b), and π^* CH_3 (c) molecular orbitals in the gas phase, and onefold and twofold adsorbed on Rh(111). The Fermi level is indicated by E_F.

TABLE 3b

Gross Population Extended Hückel of CH_3 Adsorbed on Rh(111) and Ni(111)

Orbital	Free	Rh(111)		Ni(111)	Ni(111)[a]
		Atop	Bridge	Atop	Atop
π^*	0.0	0.011	0.012	0.014	0.009
n	0.5	0.744	0.703	0.915	0.916
π	1.0	0.998	0.994	0.996	0.996

[a] d orbital parameter changed.

orbital. The metal p_y and d_{yz} orbitals are antisymmetrical with respect to the xz plane, and their interaction with the n CH_3 orbital will be small. Since the n CH_3 orbital is not perfectly symmetric these interactions are small and not zero. The $d_{x^2-y^2}$ orbital is a special case since it is symmetric with respect to both the yz and the xz planes. However, two lobes are positive and two are negative while the n CH_3 orbital is completely positive and their interaction will be zero.

These geometric considerations are completely in line with calculated bond order overlap populations. A large population is found for interaction of the n CH_3 orbital with the metal s (0.194), p_z (0.203), and d_{z^2} (0.169) orbitals. Zero interaction is found for interaction with the metal p_x, $d_{x^2-y^2}$, d_{xy}, and d_{xz} orbitals while interactions with the p_y and d_{yz} orbitals are about $1\ 10^{-6}$.

In Fig. 6a calculated bond order densities are plotted of the n CH_3 orbital with the s, p_z, and d_{z^2} orbitals of the bonding surface Rh atom in case of onefold adsorption. All three interactions are strongly bonding (see Table 4), but also large differences are found. For the interaction of the n CH_3 orbital with the metal s orbital we see that up to -9.4 eV bonding interactions are found, and for higher energies antibinding levels also become filled. Since the Fermi level of the Rh cluster is at -10.99 eV, only bonding levels are filled. In case of interaction of the n CH_3 orbital with the metal p_z orbital bonding levels are found up to -4.9 eV. In both cases an increase of the valence electron occupation would strengthen the metal–CH_3 interaction. This is in contrast with the interaction of the n CH_3 orbital with the metal d_{z^2} orbital, which has antibonding levels from -12.4 eV and higher. This means that some antibonding levels are occupied, and increasing the Rh valence electron occupation would weaken this bonding interaction. In all three plots a small density peak is found at about -24.33 eV, originating from interaction with the σ orbital of CH_3 (energy in gas phase: -24.08 eV).

Since the two degenerate π^* orbitals have a different symmetry with respect to the Rh–Rh axis, we discuss them separately. It must be noted beforehand that interactions

TABLE 4

Bond Order Overlap Population between CH_3 and Surface Group Orbitals of Rh(111)

	Rh(111)		
	Atop	Bridge symmetry	
		σ	π
$s - \pi^*CH_3$	0.00	$0.66\ 10^{-3}$	$0.39\ 10^{-3}$
$s - n\ CH_3$	0.194	0.162	0.00
$p_x - \pi^*CH_3$	$0.84\ 10^{-3}$	$0.77\ 10^{-4}$	$0.59\ 10^{-3}$
$p_x - n\ CH_3$	0.00	0.108	0.00
$p_y - \pi^*CH_3$	$0.75\ 10^{-3}$	$0.90\ 10^{-3}$	$0.85\ 10^{-3}$
$p_y - n\ CH_3$	0.00	$0.30\ 10^{-4}$	0.00
$p_z - \pi^*CH_3$	0.00	$-0.65\ 10^{-4}$	$-0.19\ 10^{-2}$
$p_z - n\ CH_3$	0.203	$0.81\ 10^{-1}$	0.00
$d_{x^2-y^2} - \pi^*CH_3$	$0.54\ 10^{-3}$	$0.35\ 10^{-6}$	$0.73\ 10^{-5}$
$d_{x^2-y^2} - n\ CH_3$	0.00	$0.31\ 10^{-1}$	0.00
$d_{z^2} - \pi^*CH_3$	0.00	$0.35\ 10^{-2}$	$0.26\ 10^{-2}$
$d_{z^2} - n\ CH_3$	0.169	$0.11\ 10^{-1}$	0.00
$d_{xy} - \pi^*CH_3$	$0.58\ 10^{-3}$	$0.39\ 10^{-2}$	$0.13\ 10^{-4}$
$d_{xy} - n\ CH_3$	0.001	$0.14\ 10^{-5}$	0.00
$d_{xz} - \pi^*CH_3$	$0.11\ 10^{-1}$	$0.41\ 10^{-3}$	$0.81\ 10^{-2}$
$d_{xz} - n\ CH_3$	0.00	0.136	0.00
$d_{yz} - \pi^*CH_3$	$0.11\ 10^{-1}$	$0.23\ 10^{-2}$	$0.48\ 10^{-2}$
$d_{yz} - n\ CH_3$	0.00	$0.47\ 10^{-4}$	0.00

Note. In case of twofold adsorption, CH_3 is adsorbed on a site consisting of two Rh atoms aligned along the x-axis and perpendicular to the surface along the z-axis. σ and π indicate symmetry and antisymmetry with respect to the yz mirror plane.

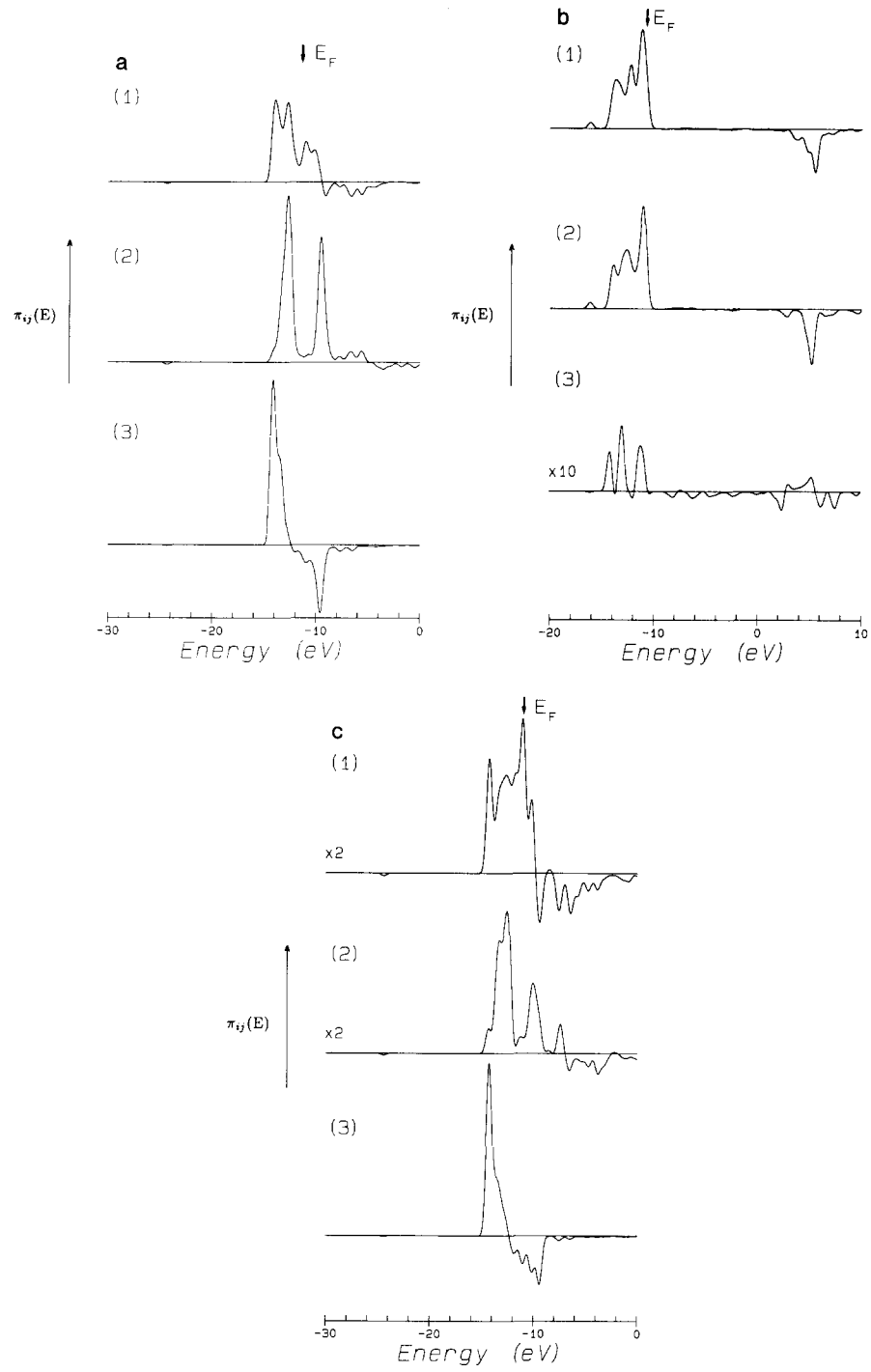

FIG. 6. Bond order overlap population densities of CH_3 with surface metal orbitals on Rh(111). (a) CH_3 adsorbed onefold on Rh(111); (1) n CH_3 − s; (2) n CH_3 − p_z; (3) n CH_3 − d_{z^2}. (b) CH_3 adsorbed onefold on Rh(111): (1) π^* − d_{xz}; (2) π^* − d_{yz}; (3) π^* − $d_{x^2-y^2}$. (c) CH_3 adsorbed twofold on Rh(111): (1) n CH_3 − $[1/\sqrt{2 + 2S}\,(s(1) + s(2))]$; (2) n CH_3 − $[1/\sqrt{2 - 2S}\,(p_x(1) - p_x(2))]$; (3) n CH_3 − $[1/\sqrt{2 - 2S}\,(d_{xz}(1) - d_{xz}(2))]$.

of the π^* orbitals with Rh orbitals will be much smaller than interactions of the n CH_3 orbital. In the LDOS results of CH_3 a small population of the π^* orbitals is seen in comparison with a considerable population of the n CH_3 orbital. First we look at interactions involving the π^* orbital formed out of the carbon p_x and two hydrogen s orbitals (Fig. 4b). Since this orbital is perfectly antisymmetric with respect to the yz plane, the interaction with symmetric metal orbitals (the s, p_y, $d_{x^2-y^2}$, d_{z^2}, and d_{yz} orbitals) will be zero. The π^* orbital is not perfectly symmetric with respect to the xz plane. Both the metal p_x and d_{xz} orbitals are (perfectly) symmetric with respect to the xz plane (and antisymmetric with respect to the yz plane), and will have a strong interaction with the π^* CH_3 orbital. The d_{xy} orbital is antisymmetric with respect to the xz plane, and will hardly interact with the π^* CH_3 orbital.

The other π^* orbital is formed from a combination of the carbon p_y orbital with three hydrogen s orbitals, and is perfectly symmetric with respect to the yz plane. Interaction with metal orbitals which are antisymmetric relative to the yz plane (the p_x, d_{xz}, and d_{xy} orbitals) will be zero. This π^* CH_3 orbital is locally not perfectly antisymmetric with respect to the xz plane. As the metal s, p_z, d_{z^2}, and $d_{x^2-y^2}$ orbitals are symmetric relative to the xz plane, their interaction with the π^* CH_3 orbital will be small. The metal p_y and d_{yz} orbitals are perfectly antisymmetric with respect to the xz plane (and symmetric with respect to the yz plane) and will have a strong interaction with the π^* CH_3 orbital.

Calculated bond order overlap populations can be found in Table 4. In the case of interaction of the π^* CH_3 orbitals with surface metal orbitals, only interaction with one of the two π^* orbitals is possible and the other interaction will be zero. Table 4 lists only the nonzero value. The π^* orbitals mainly bond with the d_{xz} and d_{yz} orbitals. As mentioned before, their bond order overlap populations (0.11×10^{-1}) are considerably smaller than bond order populations of surface metal orbitals with the n CH_3 orbital.

Figure 6b gives bond order overlap densities of interaction of metal orbitals with the π^* orbitals of CH_3. The calculated densities of the d_{xz} and d_{yz} orbitals interacting with the π^* orbitals are quite similar, as can be expected from geometric reasons and calculated bond order populations (Table 4). The bond order overlap density of the interaction of the $d_{x^2-y^2}$ orbital with the π^* orbitals is much smaller. Both the π^* CH_3 (Fig. 4c) and $d_{x^2-y^2}$ orbitals are symmetric with respect to the yz plane. Differences in symmetry with respect to the xz plane result in an interaction which is small but not zero. The small density peak at about -16.14 eV originates from interaction with the π CH_3 orbitals (gas phase energy: -16.08 eV).

Local density of states plots of relevant surface metal orbitals (the s, p_z, d_{z^2}, and d_{xz} orbitals) before and after onefold adsorption of CH_3 are given in Fig. 7. Atomic orbital gross populations are given in Table 3a. The metal s, p_z, and d_{z^2} orbitals have interaction with the n CH_3 orbital. The density at -24.33 eV originates from interaction with the σ CH_3 orbital. The metal d_{xz} orbital interacts with the π^* CH_3 orbital. Interaction with the π CH_3 orbitals results in a density peak at -16.14 eV.

Both the s (0.293) and p_z (0.113) orbitals are hardly populated before adsorption, while the d_{z^2} (0.922) and d_{xz} (0.891) orbitals are almost completely occupied. The atomic gross populations of the s and p_z orbitals are increased considerably after adsorption to 0.460 and 0.304, respectively. Density is pushed below the Fermi level (Figs. 7a and 7b) due to interaction with the n CH_3 orbital. In case of the d_{z^2} orbital, density is pushed above the Fermi level (Fig. 7c) and the gross population decreases to 0.710. As a result repulsion between the highly occupied d_{z^2} orbital and the half-occupied n CH_3 orbital is decreased. This corresponds to the bond order overlap density results discused above. In the case of interaction of the n

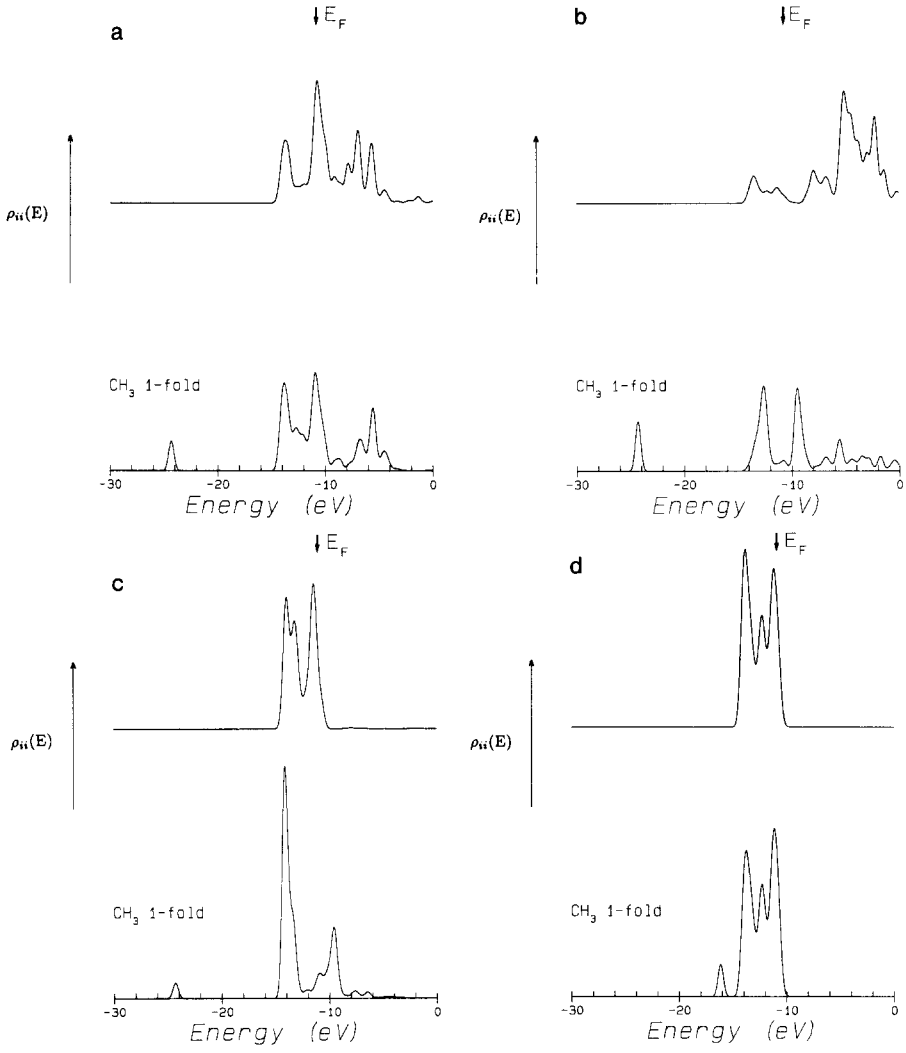

FIG. 7. LDOS of Rh s (a), p_z (b), d_{z^2} (c), and d_{xz} (d) before and after onefold adsorption of CH_3 on Rh(111).

CH_3 orbital with the s and p_z orbitals only bonding levels are occupied, while in the case of interaction with the d_{z^2} orbital antibonding levels are occupied from -12.36 eV up to higher energies. This also explains that the LDOS of the n CH_3 orbital is split into a bonding and an antibonding peak (Fig. 5b).

The atomic orbital gross population of the d_{xz} orbital is slightly decreased from 0.891 to 0.869. This corresponds to a small electron donation to the π^* orbitals of CH_3. We have seen in the LDOS of the π^* orbitals that the atomic gross population of the π^* CH_3 orbitals is increased from 0.0 to 0.011 upon onefold adsorption of CH_3.

In the next section we consider adsorption of CH_3 on a twofold site. Arbitrarily we have chosen this site to be along the x-axis. Group orbitals are constructed by taking the combination of two metal atomic orbitals. In this way we can construct group orbitals

which are symmetric and group orbitals which are antisymmetric with respect to a yz plane through the C atom of CH_3. For example,

$$\Phi^{2f}(d_{z^2}) = \frac{1}{\sqrt{2 + 2S}}(d_{z^2}(1) + d_{z^2}(2))$$

is symmetric and

$$\Phi^{2f}(d_{z^2}) = \frac{1}{\sqrt{2 - 2S}}(d_{z^2}(1) - d_{z^2}(2))$$

is antisymmetric. However,

$$\Phi^{2f}(d_{xz}) = \frac{1}{\sqrt{2 + 2S}}(d_{xz}(1) + d_{xz}(2))$$

is also antisymmetric. S is the orbital overlap.

Again some general rules can be derived. While for onefold adsorption of CH_3 the position of metal and CH_3 orbitals are the same in the xy plane, CH_3 is in between two metal atoms on the x-axis for twofold coordination. This results in less strict symmetry conditions relative to the xz plane for interaction of metal (group) orbitals with the π^* CH_3 orbitals. We discuss interaction with the n CH_3 and both π^* orbitals separately.

Group orbitals which are antisymmetric with respect to the yz plane will have no interaction with the n CH_3 orbital since this orbital is perfectly symmetric. Symmetric group orbitals will have a strong interaction with the n CH_3 orbital only when they are also symmetric with respect to the xz plane. The σ type group orbitals of the s, p_x, p_z, $d_{x^2-y^2}$, d_{z^2}, and d_{xz} orbitals fulfill this condition. The symmetric group orbitals which are antisymmetric with respect to the xz plane (the p_y, d_{xy}, and d_{yz} orbitals) will have a small interaction with the n CH_3 orbital. Since the n CH_3 orbital is not perfectly symmetric with respect to the xz plane these interactions are small and not zero. This is confirmed by Table 4, where we see large bond order overlap populations in the case of interaction of the n CH_3 orbital with the symmetric s (0.162), p_x (0.108), and d_{xz} (0.136) orbitals. These bond order overlap populations are plotted in Fig. 6c. The electron occupancy of the symmetric s orbital (Table 3a) increases from 0.327 to 0.485, that of the p_x orbital from 0.163 to 0.232. The interaction of the n CH_3 orbital with the symmetric d_{xz} orbital results in a repulsion as the symmetric d_{xz} orbital is almost completely occupied. The occupation is decreased from 0.948 to 0.815 in order to decrease repulsion by pushing density above the Fermi level. The bond order populations of the symmetric p_z, $d_{x^2-y^2}$, and d_{z^2} orbitals are small, while interactions of antisymmetric group orbitals are zero. Changes in metal atomic gross orbital population (Table 3a) are small.

We discuss now interaction of metal group orbitals with the π^* orbital of CH_3 which is a combination of the carbon p_x and two hydrogen s orbitals (see Fig. 4b). This π^* orbital is antisymmetric relative to the xz plane. Interaction with surface metal group orbitals which are symmetric will be zero; interaction of group orbitals which are antisymmetric is possible.

The second π^* CH_3 orbital is a combination of three hydrogen s orbitals with the carbon p_y orbital, and is symmetric with respect to the yz plane (Fig. 4c). Interaction with σ type metal group orbitals is possible; interaction with π type metal group orbitals will be zero.

Metal group orbitals will always have interaction with one of the π^* orbitals and calculated bond order overlap populations will never be zero. This is confirmed by Table 4. Since the overall interaction of the π^* CH_3 orbitals with the metal surface is small (because of the large energy difference), bond order populations are considerably smaller than interactions of the surface with the n CH_3 orbital.

The onefold adsorption of CH_3 is dominated by interactions of the n CH_3 orbital with the metal s, p_z, and d_{z^2} orbitals, while interactions of the n CH_3 orbital with the symmetric s, p_x, and d_{xz} orbitals are important in the case of twofold adsorption. Interaction with the π^* orbitals is small in both

cases. When we compare relevant bond order overlap populations of onefold (Fig. 6a) and twofold (Fig. 6c) adsorbed CH_3, we see that at high energy the ratio of antibonding to bonding interactions is higher in the case of twofold adsorption. Therefore, at high valence electron occupation, more antibonding levels are occupied for twofold adsorption and CH_3 will adsorb on onefold sites. This is in agreement with the ASED results presented in Figs. 1e and 1f.

Combination Reaction of CH_3 and CH_2 on Rh(111)

Methane and hydrocarbons can be produced from synthesis gas by Fischer–Tropsch catalysts such as Fe, Ni, Co, and Ru (*4, 73*). Under reaction conditions, a reactive CH_x species is formed on the metal surface, which is involved in a number of processes such as insertion (resulting in longer hydrocarbon chains) and termination reactions (hydrogenation or hydrogen abstraction).

For each step of the Fischer–Tropsch synthesis a specific reaction can be studied with quantum chemical methods as an example. Because of the large number of parameters (choice of adsorption sites, length of carbon chain of interacting hydrocarbon fragments, intramolecular and intermolecular carbon–hydrogen and carbon–carbon distances) even a thorough study of one single reaction is an enormous task. The ASED molecular orbital method can be used since it allows a large number of calculations and geometry optimization. Zheng *et al.* (*55*) have studied coupling of C_1 fragments with the extended Hückel method. In their approach specific reaction paths for propagation and termination reactions are assumed.

When the distance between adsorbed molecules is reduced they begin to influence each other, resulting in repulsive and attractive forces. When the attractive forces prevail, a reaction will take place, but when they are exceeded by repulsive ones, the result will be a repulsion between the molecules. We have started our study of the combination reaction of CH_3 and CH_2 (a propagation reaction) with the coadsorption of CH_3 and CH_2.

CH_3 and CH_2 are coadsorbed on Rh(111) in six different geometries, which are plotted in Fig. 8. One of the molecules is fixed at a certain site at the optimized height when adsorbed alone on the surface (see Table 1). The height of the other molecule is optimized in steps of 0.1 Å. This calculation is repeated by fixing the height of the second molecule and optimizing the height of the first one. Results are given in Table 5. In a number of cases there is a (local) minimum in energy at a small distance to the surface, while increasing the height to very large distances still results in a lowering of the energy (an increase of the adsorption energy). In these cases Table 5 also gives the adsorption energy for the largest distance the adsorption energy is calculated. This is indicated by listing the value of the optimized height by $>$.

A very small intermolecular distance of CH_3 and CH_2 (conformations I–IV) results in a strong repulsion, which can be attributed to steric repulsion. As can be seen in Fig. 8, these conformations result in very small intermolecular hydrogen distances. When the height of CH_2 is optimized, we find heights considerably smaller than for adsorption of CH_2 alone. For conformation I the optimized height of coadsorbed CH_2 on a twofold site is 1.2 Å, which is a decrease of 0.4 Å. We find an ASED energy E_{tot} of 3.95 eV and an extended Hückel energy E_{att} of -2.66 eV. Since the ASED energy is a summation of the extended Hückel energy E_{att} and a repulsive energy E_{rep}, a high value of E_{att} and a small (or even positive) value of E_{tot} is a strong indication that the repulsive energy is considerable.

For conformations III and IV the decrease of the CH_2 adsorption height is 0.5 Å (from 1.5 to 1.0 Å) and 0.4 Å (from 1.5 to 1.1 Å), respectively. In both cases we find a combination of a high value of E_{att} and a small value of E_{tot}, indicating strong repulsion as discussed for conformation I. Conformations III and IV only differ in the

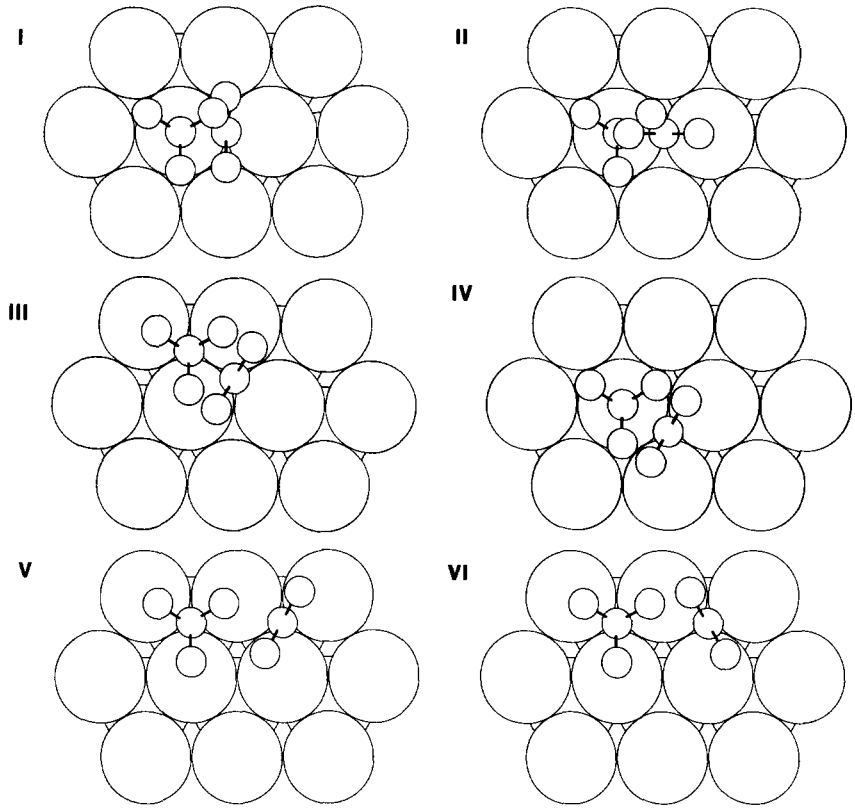

FIG. 8. Adsorption geometries of CH_3 and CH_2 coadsorbed on Rh(111).

choice of adsorption sites. In III both CH_3 and CH_2 are adsorbed on three fold sites, in IV CH_3 is adsorbed 1-fold (the preferred site) and CH_2 on a threefold site. Conformation IV is more stable than conformation III. In case of conformations III and IV the adsorption energy is calculated up to CH_2 heights of 2.4 and 2.5 Å. Increasing the height still further (which is a desorption process) results in a continuously decreasing repulsion, indicating that CH_2 is not stable and is forced to desorb.

This conclusion also holds when the height of CH_3 is optimized. For conformation I both E_{tot} and E_{att} are positive at a height of 2.5 Å, indicating that adsorption is not favorable even at this height. For the conformations II, III, and IV we find bonding interactions (E_{tot} and E_{att} are negative) but only at heights of 4.0 Å (conformation II), 3.0 Å (III), and 3.2 Å (IV) or higher, which are not realistic adsorption values.

At a distance of 2.687 Å stable geometries (conformations V and VI) are found. Both ASED energy E_{tot} and extended Hückel energy E_{att} indicate that bonding and optimized adsorption heights are (nearly) identical to adsorption of CH_3 and CH_2 alone. The same adsorption energies are found irrespective of optimization of the height of CH_3 or of CH_2.

Zheng *et al.* (*55*) indicate three stages in the reaction of two hydrocarbon molecules. The first one is a surface migration of the molecules, and the third stage is the actual reaction for which specific reaction paths are assumed. In the intermediate step the reacting fragments must come to neighboring sites. The energy involved in this step is called proximity energy (PE), which can be

TABLE 5

Coadsorption of CH_3 and CH_2 on Rh(111)

Conformation	Site CH_3	Site CH_2	d^a (Å)	Molecule varied	$h(X)^b$ (Å)	E_{tot} (eV)	E_{att} (eV)
I	1-fold	2-fold	1.343	CH_2	1.2	3.95	−2.66
I	1-fold	2-fold	1.343	CH_3	>2.5	3.08	0.20
II	1-fold	2-fold	1.343	CH_3	>4.0	−2.87	−3.87
III	3-fold hcp	3-fold fcc	1.550	CH_2	1.0	3.42	−3.16
					>2.4	4.11	1.98
III	3-fold hcp	3-fold fcc	1.550	CH_3	1.3	4.63	−1.96
					>3.0	−2.08	−3.17
IV	1-fold	3-fold hcp	1.550	CH_2	1.1	−0.02	−5.07
					>2.5	4.46	1.93
IV	1-fold	3-fold hcp	1.550	CH_3	>3.2	−2.71	−3.73
V	3-fold hcp	3-fold hcp	2.687	CH_2	1.5	−4.14	−5.39
V	3-fold hcp	3-fold hcp	2.687	CH_3	2.0	−4.14	−5.30
VI	3-fold hcp	3-fold hcp	2.687	CH_2	1.5	−3.61	−5.00
VI	3-fold hcp	3-fold hcp	2.687	CH_3	2.1	−3.68	−4.88

[a] Distance between the adsorption sites.

[b] Optimized height after variation of indicated molecule. The other molecule is kept immobile at optimized height when adsorbed alone.

defined as the energy of fragments on two adjacent sites minus the sum of adsorption energies of the two fragments. Adsorbed fragments on adjacent sites are found in our calculations in conformations V and VI, when CH_2 and CH_3 are separated by the Rh–Rh internuclear distance of 2.687 Å. Conformation V is clearly favored over conformation VI, which is another indication that the repulsion of CH_2 and CH_3 originates mainly from steric interactions of the hydrogen atoms. Conformation V results in adsorption energies of −4.14 eV (E_{tot}) and −5.39 (E_{att}). The sum of adsorption energies of threefold hcp CH_3 and CH_2 is −4.93 eV (E_{tot}) and −6.10 eV (E_{att}). Thus for Rh we find proximity energies of +0.79 eV and +0.80 eV. Zheng *et al.* give PE values of −.0.2 eV for Ti (internuclear distance of 2.95 Å), +0.8 eV for Cr (2.88 Å), and +1.2 eV for Co (2.51 Å), which agree well with our +0.80 eV for Rh (2.687 Å).

Decreasing the distance between CH_2 and CH_2 results in an increasing repulsion (Table 5), and the recombination reaction into adsorbed C_2H_5 is not favorable. However, since this repulsion is mainly due to hydrogen steric interactions, a coupling reaction might be possible when during the reaction hydrogen atoms bend away from each other in other to relieve repulsion. A second possibility is that hydrocarbon fragments with less hydrogen atoms combine, followed by a hydrogenation step to give adsorbed C_2H_5. More calculations are necessary to evaluate these reactions.

Adsorption of CH_x on Ni(111)

Several theoretical studies of CH_n (n = 1–3) on metal surfaces exist. Zheng *et al.* (*55*) studied extensively the adsorption of CH, CH_2, and CH_3 on Ti(0001), Cr(110), and Co(0001) and found that CH_x is adsorbed on a $(4 - x)$fold site in order to restore missing C–H bonds. Therefore CH is adsorbed on threefold sites, CH_2 on twofold sites, and CH_3 on threefold sites. Minot *et al.* (*54*) found similar results for adsorption of CH_x on Pt(111). Gavezzotti *et al.* (*50*) made an elaborate study of acetylene adsorption on Pt(111), and found a preference of CH for the threefold site. Later they found the same preference for CH on Rh (*51*). All these results are completely in line with our results as discussed above. In contrast with this are the results of the studies of Gavin *et al.* (*63*) and Schüle *et al.* (*57*). Gavin *et al.* (*63*) studied adsorption on Ni(111) and found that both CH and CH_3 are adsorbed on threefold sites, and CH_2 is adsorbed on twofold sites. In all the studies mentioned so far (*50, 54, 55, 64,* this study) extended Hückel methods are applied. Schüle *et al.* (*57*) used ab initio methods with configuration interaction. Calculated adsorption energies of CH_3 on Ni(111) showed a slight preference for adsorption on the threefold hollow site. However, the energy difference for different adsorption sites was smaller than the accuracy in the calculations and a definite assignment for the threefold site was made only after calculations of C–H frequencies and comparison with experimental results.

In order to study the origin of the differences between ab initio and extended Hückel calculations, we have studied adsorption of CH_x (x = 1 − 3) on Ni(111). The cluster geometry is exactly the same as that

TABLE 6a

Adsorption of CH_x on a Ni(*18,11*) Cluster Modeling a Ni(111) Surface

Species	Site	E_{tot} (eV)	E^a_{att} (eV)	E^b_{rott} (eV)	h^c_X (Å)
H	1-fold	−4.83	−5.66		1.6
	2-fold	−4.45	−5.46		1.2
	3-fold fcc[d]	−4.41	−5.34		1.1
	3-fold hcp[e]	−4.43	−5.36		1.1
C	1-fold	−8.38	−8.53		2.2
	2-fold	−8.38	−9.55		1.5
	3-fold fcc[d]	−8.59	−9.85		1.4
	3-fold hcp[e]	−8.74	−9.99		1.4
CH	1-fold	−6.61	−7.05		2.0
	2-fold	−7.20	−8.96		1.4
	3-fold fcc[d]	−7.56	−9.38		1.3
	3-fold hcp[e]	−7.72	−9.54		1.3
CH_2	1-fold	−5.55	−6.00	0.01	2.0
	2-fold	−6.27	−7.51	1.46	1.5
	3-fold fcc[d]	−5.66	−6.61	0.03	1.5
	3-fold hcp[e]	−5.73	−6.69	0.00	1.5
CH_3	1-fold	−4.47	−5.27	0.01	1.9
	2-fold	−4.24	−4.90	0.01	1.7
	3-fold fcc[d]	−4.22	−4.94	0.24	1.6
	3-fold hcp[e]	−4.23	−4.95	0.23	1.6

[a] Bond energy contribution excluding the two-body repulsion term.

[b] Difference in maximum and minimum total energy during rotation.

[c] Height of adsorbing species (X = C, H, or CH_x) above the surface.

[d] No Ni present in second layer.

[e] Ni present in second layer.

used for calculations involving Rh(111). A Ni–Ni internuclear distance of 2.4916 Å is used. ASED adsorption energies E_{tot} and extended Hückel energies E_{att} are listed in Table 6a. ASED calculations of the adsorption energy of CH_3 on Ni(111) are considerably higher (from −4.22 eV for threefold adsorption up to −4.49 eV for onefold adsorption) than results of ab initio calculations by Schüle *et al.* (*57*). In general hydrogen and CH_x are adsorbed on the same sites as on Rh(111). Atomic hydrogen prefers onefold sites, C prefers threefold hcp sites, and CH_x is found at $(4 - x)$fold sites. When we compare the difference between highest and lowest adsorption energy on Rh(111) and on Ni(111), we see that for adsorption of CH_2 this difference is larger on Ni, for H and CH it is slightly larger for Ni, and for CH_3 and C it is larger on Rh.

One of the characteristics of the extended Hückel method is the parameter dependency of the results. This can be a disadvantage, but it can also be used to study various properties by varying a single parameter. In our studies we use a double ζ basis for the d orbitals of metal atoms. In order to study the relevance of the interaction with the d valence electron band, we have changed ζ_2 of Ni from 2.0 (see Appendix) to slightly lower (1.9) and highter (2.2) values. Increasing ζ_2 results in a shift from a onefold site to higher adsorption sites (Table 6b). $\zeta_2 = 2.2$ results in a clear preference for the threefold site over lower coordination sites. In order to investigate this we have calculated bond order overlap populations for onefold and twofold adsorption for ζ_2 values of 2.0 and 2.2. Results are given in Tables 7a and 7b.

What exactly will happen when we increase the orbital exponent ζ_2? In the ASED method Slater-type orbitals are used, and the dependence of the wavefunction on the distance r from the nucleus is given by $\exp[-\zeta r]$. Increasing ζ_2 results in a decrease of the spatial extension of d orbitals, and their overlap with neighbors will also decrease. Less overlap means less interaction; the metal d band will be smaller and interaction with adsorbing molecules will decrease.

In Fig. 9a the adsorption energy of CH_3 on one-, two-, and threefold sites is plotted as a function of the number of valence electrons relative to Ni ($\zeta_2 = 2.2$) with the rigid band model. At low valence electron occupation the threefold sites (both fcc and hcp) are clearly favored over two- and onefold sites. At higher electron occupation the adsorption energy of onefold CH_3 increases while the adsorption energy on other sites decreases. The ratio of one adsorption energy of site x (two- and threefold) relative to

TABLE 6b

Influence of Ni *d* Orbital Exponent ζ_2 on Adsorption Site of CH_3

ζ_2	Site	E_{tot} (eV)	E_{att}^a (eV)	h_X^b (Å)
1.9	1-fold	−4.41	−4.88	2.0
	2-fold	−4.01	−4.67	1.7
	3-fold fcc[c]	−3.96	−4.44	1.7
	3-fold hcp[d]	−3.95	−4.43	1.7
2.0	1-fold	−4.47	−5.27	1.9
	2-fold	−4.24	−4.90	1.7
	3-fold fcc[c]	−4.22	−4.94	1.6
	3-fold hcp[d]	−4.23	−4.95	1.6
2.1	1-fold	−4.49	−5.29	1.9
	2-fold	−4.41	−5.06	1.7
	3-fold fcc[c]	−4.43	−5.15	1.6
	3-fold hcp[d]	−4.47	−5.19	1.6
2.2	1-fold	−4.49	−5.29	1.9
	2-fold	−4.52	−5.18	1.7
	3-fold fcc[c]	−4.58	−5.30	1.6
	3-fold hcp[d]	−4.64	−5.36	1.6

[a] Bond energy contribution excluding the two-body repulsion term.

[b] Height of adsorbing species (X = C, H, or CH_x) above the surface.

[c] No Ni present in second layer.

[d] Ni present in second layer.

the onefold site (denoted as E ($xf/1f$)) is given in Fig. 9b. All ratios are continuously decreasing for higher valence electron occupation. The same trends are found for CH_3 adsorption on Rh(111) (see Fig. 1e and 1f), with the exception that on Rh(111) the onefold site is favored.

In Tables 7a and 7b the bond order overlap populations are given in the case of ζ_2 = 2.0 and 2.2, respectively. Relevant bond order overlap populations in the case of ζ_2 = 2.2 are plotted in Fig. 10. Clearly, the weaker interaction with the metal *d* band is confirmed. CH_3 adsorption on two- and threefold sites show the same trends in adsorption energy (Table 6b). We have discussed in a previous section that adsorption of CH_3 is mainly a result of σ type interactions of surface metal orbitals with the *n* CH_3 orbital. This orbital is considerably more populated after adsorption on Ni(111) (gross population of 0.915) than when adsorbed on Rh(111) (0.703). Figure 11 shows the LDOS of CH_3 onefold adsorbed on Ni(111) with ζ_2 = 2.2. We find that an increase of ζ_2 results in a small increase of gross population of the *n* CH_3 orbital and a small decrease of gross population of the π^* orbitals (Table 3b). From a comparison of Tables 7a and 7b we find an increase of overlap populations of metal *s* orbitals (and to a lower extent *p* orbitals), and a decrease in overlap populations of metal *d* orbitals. Due to the smaller spatial extension of the *d* orbitals the overlap with the *n* orbital of CH_3 will be smaller and interaction will be less. This is also clear

TABLE 7a

Bond Order Overlap Population between CH_3 and Surface Group Orbitals of Ni(111)

	Ni(111)		
	Atop	Bridge symmetry	
		σ	π
s − π^*CH_3	0.00	$0.76\ 10^{-3}$	$-0.26\ 10^{-3}$
s − *n* CH_3	0.265	0.220	0.00
p_x − π^*CH_3	$0.29\ 10^{-4}$	$0.49\ 10^{-3}$	$0.17\ 10^{-2}$
p_x − *n* CH_3	0.00	0.211	0.00
p_y − π^*CH_3	$-0.30\ 10^{-3}$	$0.12\ 10^{-3}$	$0.36\ 10^{-2}$
p_y − *n* CH_3	0.00	$0.31\ 10^{-4}$	0.00
p_z − π^*CH_3	0.00	$-0.92\ 10^{-4}$	$-0.12\ 10^{-2}$
p_z − *n* CH_3	0.213	$0.84\ 10^{-1}$	0.00
$d_{x^2-y^2}$ − π^*CH_3	$0.59\ 10^{-3}$	$0.11\ 10^{-4}$	$0.25\ 10^{-4}$
$d_{x^2y^2}$ − *n* CH_3	0.00	$0.21\ 10^{-1}$	0.00
d_{z^2} − π^*CH_3	0.00	$0.31\ 10^{-2}$	$0.46\ 10^{-2}$
d_{z^2} − *n* CH_3	$0.98\ 10^{-1}$	$0.40\ 10^{-2}$	0.00
d_{xy} − π^*CH_3	$0.60\ 10^{-3}$	$0.53\ 10^{-2}$	$-0.55\ 10^{-5}$
d_{xy} − *n* CH_3	0.00	$0.32\ 10^{-5}$	0.00
d_{xz} − π^*CH_3	$0.13\ 10^{-1}$	$0.38\ 10^{-3}$	$0.11\ 10^{-1}$
d_{xz} − *n* CH_3	0.00	$0.82\ 10^{-1}$	0.00
d_{yz} − π^*CH_3	$0.13\ 10^{-1}$	$0.30\ 10^{-2}$	$0.45\ 10^{-2}$
d_{yz} − *n* CH_3	0.00	$-0.89\ 10^{-5}$	0.00

Note. In case of twofold adsorption, CH_3 is adsorbed on a site consisting of two Ni atoms aligned along the *x*-axis and perpendicular to the surface along the z-axis. σ and π indicate symmetry and antisymmetry with respect to the *yz* mirror plane.

TABLE 7b

Bond Order Overlap Population between CH_3 and Surface Group Orbitals of Adapted Ni(111) (d Orbital Exponent $\zeta_2 = 2.2$)

	Adapted Ni(111)		
	Atop	Bridge symmetry	
		σ	π
$s - \pi^*CH_3$	0.00	$0.63\ 10^{-3}$	$-0.13\ 10^{-3}$
$s - n\ CH_3$	0.272	0.226	0.00
$p_x - \pi^*CH_3$	$-0.32\ 10^{-3}$	$0.17\ 10^{-3}$	$0.11\ 10^{-2}$
$p_x - n\ CH_3$	0.00	0.213	0.00
$p_y - \pi^*CH_3$	$-0.77\ 10^{-3}$	$-0.36\ 10^{-3}$	$0.22\ 10^{-2}$
$p_y - n\ CH_3$	0.00	$0.27\ 10^{-4}$	0.00
$p_z - \pi^*CH_3$	0.00	$-0.13\ 10^{-3}$	$-0.92\ 10^{-3}$
$p_z - n\ CH_3$	0.211	$0.84\ 10^{-1}$	0.00
$d_{x^2-y^2} - \pi^*CH_3$	$0.32\ 10^{-3}$	$0.42\ 10^{-5}$	$0.45\ 10^{-4}$
$d_{x^2-y^2} - n\ CH_3$	0.00	$0.15\ 10^{-1}$	0.00
$d_{z^2} - \pi^*CH_3$	0.00	$0.18\ 10^{-2}$	$0.36\ 10^{-2}$
$d_{z^2} - n\ CH_3$	$0.80\ 10^{-1}$	$0.37\ 10^{-2}$	0.00
$d_{xy} - \pi^*\ CH_3$	$0.33\ 10^{-3}$	$0.34\ 10^{-2}$	$-0.62\ 10^{-5}$
$d_{xy} - n\ CH_3$	0.00	$0.15\ 10^{-5}$	0.00
$d_{xz} - \pi^*CH_3$	$0.90\ 10^{-2}$	$0.16\ 10^{-3}$	$0.80\ 10^{-2}$
$d_{xz} - n\ CH_3$	0.00	$0.61\ 10^{-1}$	0.00
$d_{yz} - \pi^*CH_3$	$0.88\ 10^{-2}$	$0.20\ 10^{-2}$	$0.25\ 10^{-2}$
$d_{yz} - n\ CH_3$	0.00	$-0.29\ 10^{-5}$	0.00

Note. In case of twofold absorption, CH_3 is adsorbed on a site consisting of two Ni atoms aligned along the x-axis and perpendicular to the surface along the z-axis. σ and π indicate symmetry and antisymmetry with respect to the yz mirror plane.

from a comparison of the interaction of the $n\ CH_3$ orbital with the metal s and d_{z2} orbitals in case of onefold adsorption (Fig. 10a, (1) and (2)), and for twofold adsorption interaction of the $n\ CH_3$ orbital with the symmetric s and d_{xz} orbitals (Fig. 10c, (1) and (3)).

Increasing ζ_2 results in more s and less d character of the bond between the metal surface and CH_3. The strength of the M–C bond is found by a summation of all relevant bond order populations (values higher than 0.1×10^{-1}) of Tables 7a and 7b. For $\zeta_2 = 2.0$ we find total values of 0.602 and 0.629 for one- and twofold sites, respectively, and a ratio of ($2f/1f$) of 1.04. For $\zeta_2 = 2.2$ values are 0.563 (sum of onefold), 0.599 (sum of twofold), and 1.06 (ratio). For both cases the M–C bond is stronger in the case of twofold adsorption than in the case of onefold adsorption, but the ratio of bond strengths of two- to onefold sites is increased for higher ζ_2. This increased ($2f/1f$) ratio for $\zeta_2 = 2.2$ agrees with the ASED results of Table 6b, which indicates a shift from onefold to higher adsorption sites for increased values of ζ_2.

The ($2f/1f$) ratio of $\zeta_2 = 2.0$ is slightly higher than one, indicating that also in this case twofold adsorption is favored, while the total energy as calculated with ASED (Table 6b) indicates onefold adsorption. A similar case is found in a previous study of one- and twofold adsorption of CO on Rh(111) (*36*), and is due to the fact that the sum of the bond order overlap populations indicates the strength of the M–CH_3 bond only. The total ASED energy is a result of all bonds in a cluster, and includes besides the M–CH_3 bond also metal–metal bonds. In an extended Hückel study of CH_3 adsorption on metal surfaces, Zheng *et al.* (*55*) found that the M–C bond strength of the twofold site is larger than that of the onefold site, while in the case of twofold adsorption smaller M–M bond strengths were found. The overall adsorption energy favored onefold sites. The explanation was given by the $d - n\ CH_3$ (repulsive) interactions. In case of onefold adsorption both bonding and antibonding M–M levels were pushed above the Fermi level, resulting in a small change in the M–M bond. In case of twofold adsorption only bonding levels were pushed above E_F resulting in a weakening of the M–M bond.

CONCLUSIONS

Atom superposition and electron delocalization and extended Hückel MO studies are presented of adsorption of CH, CH_2, and CH_3 on Rh(111). CH_x is adsorbed on $(4 - x)$fold adsorption sites in order to restore the missing $(4 - x)$ C–H bonds. The adsorption energy of CH is higher than that of CH_2 and the adsorption energy of CH_3 the lowest. The higher adsorption energy also results in smaller adsorption heights of CH. Rigid band model calculations are presented. CH favors threefold sites regardless of the Fermi level. CH_2 favours twofold sites, but at high Fermi level onefold sites

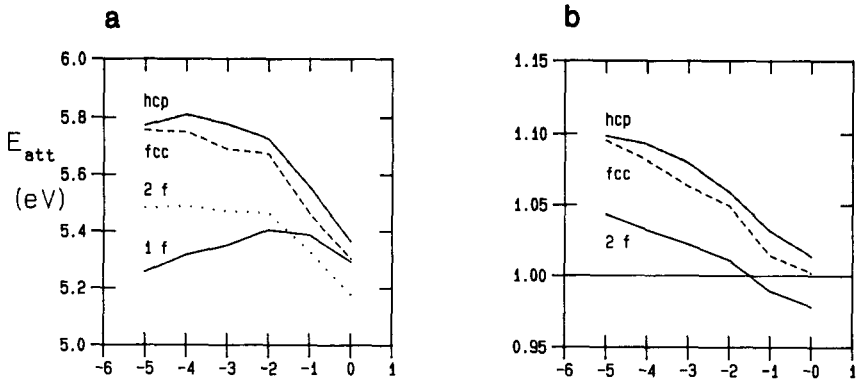

FIG. 9. Adsorption energy (E_{att}) and ratio of adsorption energy on a x-fold site to that of the onefold site ($E(xf/1f)$) of CH_3 on (111) ($\zeta_2 = 2.2$) surface as a function of number of metal valence electrons per atom compared to Ni(O). (a) E_{att} of CH_3 adsorbed onefold, twofold, threefold fcc and threefold hcp. (b) The ratio of the adsorption energy of CH_3 adsorbed on twofold and threefold sites relative to that of CH_3 adsorbed on onefold sites.

are about equally favored. CH_3 favors onefold sites, but shifts at low Fermi level to higher coordination sites.

The adsorption of CH_3 on Rh(111) is analyzed in detail. Local density of states plots of CH_3 indicate that the π and π^* orbitals are hardly involved in bonding. The n CH_3 orbital, which is half filled in gas phase CH_3, is considerably populated. Bond order overlap densities confirm that bonding is mainly a result of σ type interactions of the n CH_3 orbital with the metal surface. In the case of onefold adsorption large overlap populations are found for the interaction of the s, p_z, and d_{z^2} orbitals with the n CH_3 orbital. An increase in valence electron occupation would weaken the interaction of the d_{z^2} orbital and strengthen the interaction of the s and p_z orbitals with the n CH_3 orbital.

Preliminary results of the interaction of coadsorbed CH_3 and CH_2 are presented. Coadsorption at an internuclear distance of 2.687 Å gives a proximity energy of +0.80 eV. Smaller distances give a considerably stronger repulsive interaction, which can be attributed to hydrogen steric repulsion.

Adsorption of CH_3 on Ni(111) is studied as a function of the d atomic orbital dimension. A decrease in spatial extension of the Ni d orbitals resulted in a shift from onefold to higher coordination sites. Calculated bond order overlap populations indicated that interactions with surface metal d orbitals decrease and interactions with the s orbital increase. The M–C bond strength (found by a summation of relevant bond order overlap populations) of twofold adsorbed CH_3 relative to that of CH_3 adsorbed on onefold sites increases for smaller Ni d orbitals, indicating a preference for higher coordination sites. These results indicate that the delicate balance of s and d metal valence electron interactions with the n CH_3 orbital determines the topology of the adsorption site of CH_3.

APPENDIX

APPENDIX TABLE

Atomic Parameters: Principal Quantum Number (n), Ionization Potential (VSIP), Orbital Exponents (ζ), and Respective Coefficients (C_i) – d Used Only

Atom	s			p		
	n	VSIP	ζ	n	VSIP	ζ
C	2	20.00	1.658	2	11.26	1.618
O	2	28.48	2.246	2	13.62	2.227
Rh	5	8.09	2.135	5	4.57	2.100
Ni	4	7.63	1.800	4	4.45	1.500

	n	VSIP	ζ_1	C_1	C_2	ζ_2
Rh	4	12.50	4.290	0.5807	0.5685	1.97
Ni	3	10.00	5.750	0.5681	0.6293	2.00

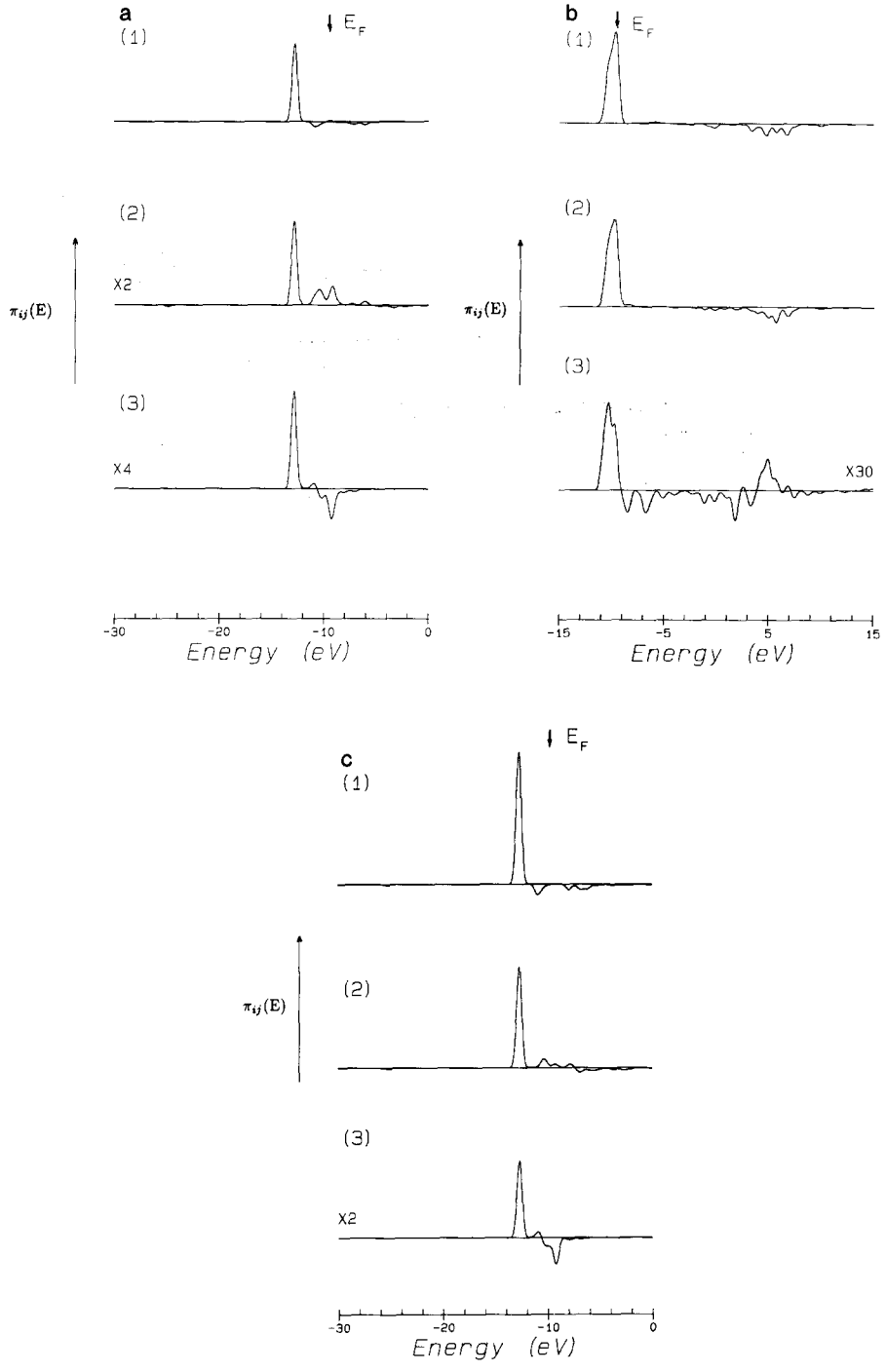

FIG. 10. Bond order overlap population densities of CH_3 with surface metal orbitals on Ni(111) (ζ_2 = 2.2). (a) CH_3 adsorbed onefold: (1) n CH_3 − s; (2) n CH_3 − p_z; (3) n CH_3 − d_{z^2}. (b) CH_3 adsorbed onefold: (1) π^* − d_{xz}; (2) π^* − d_{yz}; (3) π^* − $d_{x^2-y^2}$. (c) CH_3 adsorbed twofold: (1) n CH_3 − $[1/\sqrt{2 + 2S}\,(s(1) + s(2))]$; (2) n CH_3 − $1/\sqrt{2 - 2S}\,(p_x(1) - p_x(2))]$; (3) n CH_3 − $[1/\sqrt{2 - 2S}\,(d_{xz}(1) - d_{xz}(2))]$.

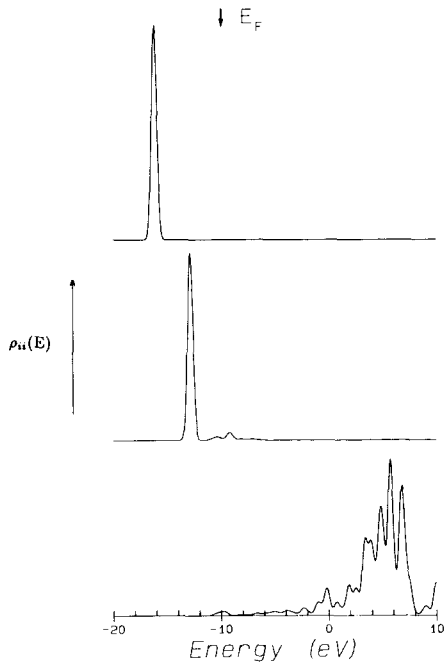

FIG. 11. LDOS of the π CH_3 (a), n CH_3 (b), and π^* CH_3 (c) molecular orbitals of CH_3 onefold adsorbed on Ni(111) (ζ_2 = 2.2). The Fermi level is indicated by E_F.

REFERENCES

1. Fischer, F., and Tropsch, H. *Ber. Dtsch. Chem. Ges.* **59,** 830 (1926).
2. Anderson, R. B., *in* "Catalysis" (P. H. Emmett, Ed.), Vol. IV. Reinhold, New York, 1956.
3. Pichler, H., and Schulz, H., *Chem. Ing. Tech.* **42,** 1162 (1970).
4. Ponec, V., *Catal. Rev. Sci. Eng.* **18,** 151 (1978).
5. Pichler, H., *Adv. Catal.* **4,** 271 (1952).
6. Eidus, Y. T., *Russ. Chem. Rev.* **36,** 338 (1967).
7. Biloen, P., Helle, J. N., and Sachtler, W. M. H., *J. Catal.* **58,** 75 (1979).
8. Brady, R. C., and Pettit, R., *J. Amer. Chem. Soc.* **102,** 6181 (1980).
9. Brady, R. C., and Pettit, R., *J. Amer. Chem. Soc.* **103,** 1287 (1980).
10. Biloen, P., and Sachtler, W. M. H., *Adv. Catal.* **30,** 165 (1981).
11. van Barneveld, W. A. A., and Ponec, V., *J. Catal.* **88,** 382 (1984).
12. Sachtler, W. M. H., *in* "Proc. 8th In. Congress on Catalysis, Berlin, 1984," Vol. 1, p. 151. Verlag Chemie, Weinheim.
13. Wentrček, P. R., Wood, B. J., and Wise, H. J., *J. Catal.* **43,** 363 (1976).
14. Rabo, J. A., Risch, A. P., and Poutsma, M. L. J., *J. Catal.* **53,** 295 (1978).
15. Sachtler, W. M. H., *Chem. Ing. Tech.* **54,** 901 (1982).
16. Dalmon, J. A., and Martin, G. A. J., *J. Catal.* **84,** 45 (1983).
17. Araki, M., and Ponec, V., *J. Catal.* **44,** 439 (1976).
18. Ponec, V., and van Barneveld, W. A. A., *Ind. Eng. Chem. Prod. Res. Dev.* **18,** 268 (1979).
19. Bell, A. T., *Catal. Rev. Sci. Ing.* **23,** 203 (1981).
20. Sung, S.-S., and Hoffmann, R., *J. Amer. Chem. Soc.* **107,** 578 (1985).
21. Anderson, A. B., and Dowd, D. Q., *J. Phys. Chem.* **91,** 869 (1987).
22. Ray, N. K., and Anderson, A. B., *Surf. Sci.* **125,** 803 (1983).
23. Mehandru, S. P., and Anderson, A. B., *Surf. Sci.* **169,** L281 (1986).
24. Mehandru, S. P., and Anderson, A. B., *Surf. Sci.* **201,** 345 (1988).
25. Garfunkel, E. L., and Feng, X., *Surf. Sci.* **176,** 445 (1986).
26. Ban, M. I., van Hove, M. A., and Somorjai, G. A., *Surf. Sci.* **185,** 355 (1987).
27. Rodriguez, J. A., and Campbell, C. T., *J. Phys. Chem.* **91,** 2161 (1987).
28. Allen, V. M., Jones, W. E., and Pacey, P. D., *Surf. Sci.* **199,** 309 (1988).
29. van Santen, R. A., *J. Mol. Catal.*, to appear.
30. Cao, P.-L., Wu, Y., Chen, Y.-Q., and Zheng, D.-J., *Appl. Surf. Sci.* **22/23,** 452 (1985).
31. Post, D., and Baerends, E. J., *J. Chem. Phys.* **78,** 5663 (1983).
32. Gavezzotti, A., Tantardini, G. F., and Miessner, H., *J. Phys. Chem.* **92,** 872 (1988).
33. Koutecky, J., Pacchioni, G., and Fantucci, P., *Chem. Phys.* **99,** 87 (1985).
34. Pacchioni, G., and Koutecky, J., *J. Phys. Chem.* **91,** (1987) 2658.
35. Yin-Sheng, X., and Xiao-Le, H., *J. Mol. Catal.* **33,** 179 (1985).
36. de Koster, A., and van Santen, R. A., manuscript in preparation.
37. de Koster, A., and van Santen, R. A., manuscript in preparation.
38. van Langeveld, A. D., de Koster, A., and van Santen, R. A., *Surf. Sci.*, in press.
39. Casalone, G., Cattania, M. G., Merati, F., and Simonetta, M., *Surf. Sci.* **120,** 171 (1982).
40. Kesmodel, L. L., Dubois, L. H., and Somorjai, G. A., *J. Chem. Phys.* **70,** 2180 (1979).
41. Koestner, R. J., and van Hove, M. A., *Surf. Sci.* **121,** 321 (1982).
42. Dubois, L. H., Castner, D. G., and Somorjai, G. A., *J. Chem. Phys.* **72,** 5234 (1980).
43. Stewart, C. N., and Ehrlich, G., *J. Chem. Phys.* **62,** 4672 (1975).
44. Silvestre, J., and Hoffmann, R., *Langmuir* **1,** 621 (1985).
45. Mehandru, S. P., and Anderson, A. B., *Appl. Surf. Sci.* **19,** 116 (1984).

46. Chu, S.-Y., and Anderson, A. B., *Surf. Sci.* **194,** 55 (1988).
47. Anderson, A. B., and Hubbard, A. T., *Surf. Sci.* **99,** 384 (1980).
48. Anderson, A. B., Kang, D. B., and Kim, Y., *J. Amer. Chem. Soc.* **106,** 6597 (1984).
49. Mehandru, S. P., Anderson, A. B., Brazdil, J. F., and Grasselli, R. K., *J. Phys. Chem.* **91,** 2930 (1987).
50. Gavezzotti, A., Ortoleva, E., and Simonetta, M., *J. Chem. Soc. Faraday Trans.* **178,** 425 (1982).
51. Gavezzotti, A., and Simonetta, M., *Surf. Sci.* **99,** 453 (1980).
52. Geurts, P., and VAN DER Avoird, A., *Surf. Sci.* **102,** 185 (1981).
53. Nakatsuji, H., Hada, M., and Yonezawa, T., *Surf. Sci.* **185,** 319 (1987).
54. Minot, C., van Hove, M. A., and Somorjai, G. A., *Surf. Sci.* **127,** 441 (1982).
55. Zheng, C., Apeloig, Y., and Hoffmann, R., *J. Amer. Chem. Soc.* **110,** 749 (1988).
56. Upton, T. H., *J. Vac. Sci. Technol.* **20,** 527 (1982).
57. Schüle, J., Siegbahn, P., and Wahlgren, U., *J. Chem. Phys.* **89,** 6982 (1988).
58. Berke, H., and Hoffmann, R., *J. Amer. Chem.Soc.* **100,** 7224 (1978).
59. Saillard, J.-Y., and Hoffmann, R., *J. Amer. Chem. Soc.* **106,** 2006 (1984).
60. Baetzold, R. C., *J. Phys. Chem.* **88,** 5583 (1984).
61. Shustorovich, E., and Bell, A. T., *J. Catal.* **113,** 341 (1988).
62. Shustorovich, E., and Bell, A. T., submitted for publication.
63. Gavin Jr., R. M., Reutt, J., and Muetterties, E. L., *Proc. Natl. Acad. Sci. USA* **78,** 3981 (1981).
64. Anderson, A. B., Grimes, R. W., and Hong, S. Y., *J. Phys. Chem.* **91,** 245 (1987).
65. Anderson, A. B., *J. Chem. Phys.* **62,** 1187 (1975).
66. Hoffmann, R., *J. Chem. Phys.* **39,** 1397 (1963).
67. Hoffmann, R., and Lipscomb, W. N., *J. Chem. Phys.* **36,** 2179 (1962); **37,** 2872 (1962).
68. C. H. MacGillavry and G. D. Rieck, Eds.), "International Tables for X-Ray Crystallography," Vol. 3, p. 282. Kynoch, Birmingham, England, 1962.
69. Fukui, F., *Science* **218,** 747 (1982).
70. Hoffmann, R., *in* "Solids and Surfaces, a Chemist's View of Bonding in Extended Structures." VCH Publishers, New York, 1988.
71. Woodward, R. B., and Hoffmann, R., *Angew. Chem. (Int. Ed.)* **81,** 797 (1969).
72. van Santen, R. A., *J. Mol. Struct.* **173,** 157 (1988).
73. Vannice, M. A., *in* "Catalysis" (J. R. Anderson and M. Boudart, Eds.), Vol. III, Chap. 3. Springer-Verlag, Berlin, 1982.